# Structures of the Small-Molecule Bcl-2 Inhibitor (BH3I-2) and Its Related Simple Model in Protonated and Deprotonated Forms

**Daisuke Kanamori, Taka-aki Okamura, Hitoshi Yamamoto, Shigeomi Shimizu,[1] Yoshihide Tsujimoto,[1] and Norikazu Ueyama***

Department of Macromolecular Science, Graduate School of Science, Osaka University, Toyonaka, Osaka 560-0043

[1]Department of Post-Genomics and Diseases, Graduate School of Medicine, Osaka University, Suita, Osaka 565-0871

Received May 24, 2004; E-mail: ueyama@chem.sci.osaka-u.ac.jp

REPRINTED FROM

Bulletin of the Chemical Society of Japan

Vol.77 No.11 2004 p.2057–2064

November 15, 2004

The Chemical Society of Japan

# Structures of the Small-Molecule Bcl-2 Inhibitor (BH3I-2) and Its Related Simple Model in Protonated and Deprotonated Forms

**Daisuke Kanamori, Taka-aki Okamura, Hitoshi Yamamoto, Shigeomi Shimizu,[1] Yoshihide Tsujimoto,[1] and Norikazu Ueyama***

Department of Macromolecular Science, Graduate School of Science, Osaka University, Toyonaka, Osaka 560-0043

[1]Department of Post-Genomics and Diseases, Graduate School of Medicine, Osaka University, Suita, Osaka 565-0871

Received May 24, 2004; E-mail: ueyama@chem.sci.osaka-u.ac.jp

3-Bromo-5-chloro-*N*-(2-chlorophenyl)-2-hydroxybenzamide (**BCNCPB–OH**) was synthesized as a model compound of the small-molecule Bcl-2 inhibitor (BH3I-2) and characterized by $^1$H NMR and IR measurements. The structures of **BCNCPB–OH** and its deprotonated form (**BCNCPB–O–NEt$_4$**) were determined by X-ray analysis. **BCNCPB–OH** has an intramolecular OH···O=C hydrogen bond and **BCNCPB–O–NEt$_4$** has an intramolecular NH···O(oxyanion) hydrogen bond in the solid and solution states. The solution structures of protonated and deprotonated BH3I-2′ (BH3I-2 analogue) were determined by $^1$H NMR, NOESY, and IR measurements. They have similar conformations to those of the corresponding model compounds. A p$K_a$ value of **BCNCPB–OH** of 5.1 is considered a very low value for phenol derivatives, suggesting the possibility that BH3I-2 binds to protein in the deprotonated form having an intramolecular NH···O(oxyanion) hydrogen bond.

BH3I-2 is a recently identified small-molecule inhibitor of the Bcl-2 family, which is a regulator of apoptotic pathways (Chart 1).[1,2] A number of inhibitors which have a salicylamide skeleton similar to BH3I-2 have been reported to inhibit various enzymes relating to the respiratory chain,[3–6] the biosynthesis of melanin,[7,8] oxidative phosphorylation,[9–11] bacterial two component systems,[12,13] and so on. Although the precise inhibitory mechanisms in many cases are vague, drug development work has indicated that electron-withdrawing substituents[12,13] and hydrophobicity[13] are needed for a high activity. The importance of the salicylamide skeleton and hydrogen bonds on it have been shown by the following evidence. In X-ray structures of the inhibitor–scytalone dehydratase complex[7] and antimycin A$_1$–cytochrome $bc_1$ complex (the chemical structure of the inhibitors are depicted in Chart 2),[3,14] hydrogen bonds between amino acid residues in the binding site and phenolic OH, amide NH, and the carbonyl group on the salicylamide moiety were found. In these structures, intramolecular OH···O=C hydrogen bonding on the inhibitor is suggested by a short distance between the phenolic oxygen and carbonyl oxygen. The analogous inhibitor, antimycin A$_3$, is also represented as an intramolecularly OH···O=C hydrogen-bonded conformation in the proposed structure of antimycin A$_3$/Bcl-xL (one of the Bcl-2 family proteins) complex.[15,16] Modifications to break intra- and/or intermolecular hydrogen bonds such as the deletion of the phenolic OH or carbonyl group,[8] methylation of the phenolic[17] or amide[4] proton, or the insertion of –CH$_2$– between the aromatic ring and carbonyl group[4] reduce the inhibitory activity. These results demonstrate that the importance of the salicylamide skeleton arises from its hydrogen bonding ability.

Suezawa et al. has reported that salicylanilide derivatives having a halogen atom (X), a hydrogen bonding acceptor, at the 3-position are in equilibrium between intramolecular

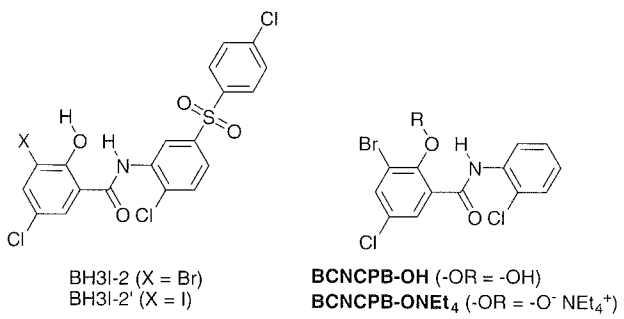


Chart 1. Chemical structures of BH3I-2, BH3I-2′, **BCNCPB–OH**, and **BCNCPB–O–NEt$_4$**.

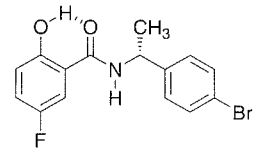


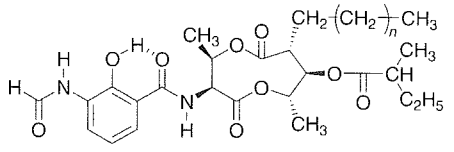


Chart 2. Other inhibitors having salicylamide moiety.

Published on the web November 11, 2004; DOI 10.1246/bcsj.77.2057

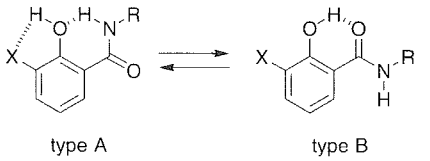


Chart 3. Two hydrogen bonding modes.

NH···O hydrogen bonded (type A) and OH···O=C hydrogen bonded conformations (type B) (Chart 3).[18] Although *O*-acetylation removes the stabilization by the intramolecular OH···O=C hydrogen bond, the type B conformation is major in solution. Salicylanilide derivatives, which can form intramolecular OH···O=C hydrogen bonds, including BH3I-2, probably favor a type B conformation. On the other hand, type A is predominant in deprotonated salicylamide derivatives by intramolecular NH···O(oxyanion) hydrogen bonds.[19,20]

The structure of the BH3I-2/Bcl-xL complex has not been determined by X-ray analysis but computationally proposed using the solution structure of the BakBH3–peptide/Bcl-xL complex.[1,21,22] In this structure, BH3I-2 binds to the hydrophobic cleft formed by BH1, BH2, and BH3 regions and takes a type A conformation depicted in Chart 1. Though it was not discussed in detail whether BH3I-2 is protonated or not, we present here the possibility of the deprotonation. The p$K_a$ values of salicylanilide derivatives have been reported below 7.5, and further lowered by electron-withdrawing substituents.[11] The p$K_a$ value of salicylamide derivatives is also reduced by the NH···O(oxyanion) hydrogen bond in its phenolate anion form.[11,19] Such intramolecular NH···O hydrogen bonds are supported in a hydrophobic environment and efficiently lower the p$K_a$ value, as shown previously in our report for thiophenol (benzenethiol) and benzoic acid analogues.[23,24] In the hydrophobic cleft of Bcl-xL, the p$K_a$ value of BH3I-2 is presumably lowered, and its deprotonated form is stabilized.

In this paper, we determine the structure of BH3I-2 and its deprotonated form and evaluate the p$K_a$ value in a hydrophobic environment using the model compounds discussed below. To realize a hydrophobic environment where BH3I-2 binds, we use organic solvents and a micellar solution.

The determination of the precise hydrogen bonding mode of BH3I-2 in the complex is important because it will be valuable for understanding inhibitory mechanisms in detail. For this purpose, 3-bromo-5-chloro-*N*-(2-chlorophenyl)-2-hydroxybenzamide (**BCNCPB–OH**) and its deprotonated form (**BCNCPB–O–NEt$_4$**) were synthesized and structurally analyzed as model compounds of protonated and deprotonated BH3I-2 (Chart 1), respectively. Because the replacement of the *N*-substituent does not significantly influence inhibitory activity, the 4-chlorophenylsulfonyl group was removed to improve the crystallinity of the BH3I-2 model compounds.[4] The structures and hydrogen bonding modes were determined by X-ray analysis and IR spectra in the solid state and by $^1$H NMR and IR spectra in solution. The structures of BH3I-2′ (Chart 1) in protonated and deprotonated forms were determined by $^1$H NMR and IR spectra in solution. The reason BH3I-2′ was employed is that it probably prefers a similar conformation to BH3I-2, which is not available commercially. To evaluate the tendency to deprotonate the phenolic OH, the p$K_a$ value of **BCNCPB–OH** was determined. The p$K_a$ value of BH3I-2 is considered to be comparable to that of **BCNCPB–OH** because introduction of a stronger electron-withdrawing group ($NO_2$) had a negligible influence on the p$K_a$ value.[11,25]

## Results and Discussion

**Synthesis.** The synthesis of **BCNCPB–OH** and **BCNCPB–O–NEt$_4$** is shown in Scheme 1. The phenolic hydroxy group was protected by an acetyl group to avoid a side reaction. The deprotonation of the phenolic OH was performed by neutralization with $NEt_4OH$.

**Structures of Model Compound in the Protonated and Deprotonated Forms in the Solid State.** The molecular structures of protonated (**BCNCPB–OH**) and deprotonated forms (**BCNCPB–O–NEt$_4$**) were determined by X-ray analy-

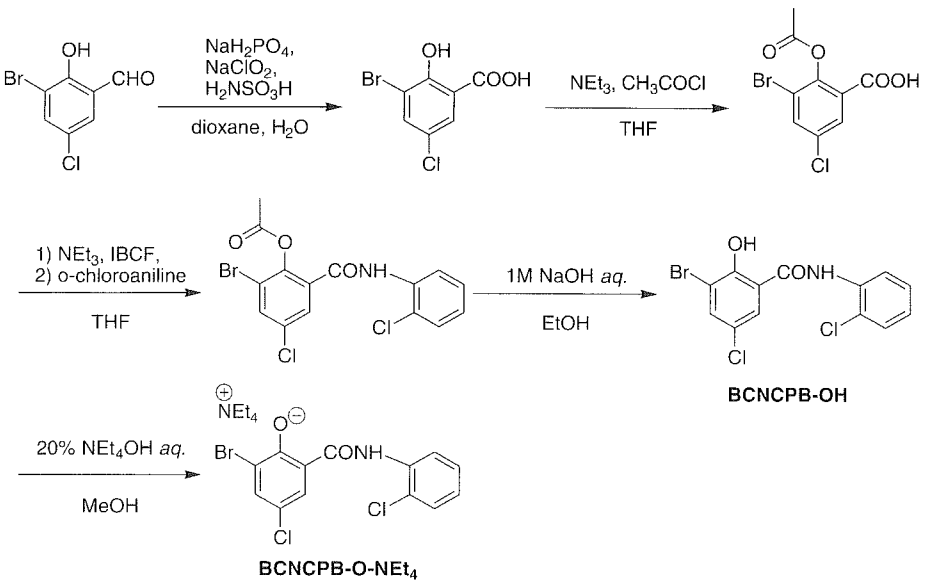


Scheme 1. Synthesis of **BCNCPB–OH** and **BCNCPB–O–NEt$_4$**. IBCF = isobutyl chloroformate.

sis. It has been revealed in the solid state that **BCNCPB–OH** prefers the type B conformation and **BCNCPB–O–NEt$_4$** prefers type A.

The molecular structure of **BCNCPB–OH** is shown in Fig. 1a and the selected short contacts, bond lengths, and torsion angles are listed in Table 1. The presence of an intramolecular OH···O=C hydrogen bond is suggested by the short distances between the phenolic OH proton (H1) and the amide carbonyl oxygen atom (O2) (1.91(3) Å) and between the phenolic oxygen (O1) and O2 (2.606(3) Å). The chlorine atom at the 2′-position in Ar$_B$ (Cl2) is located on the opposite side of the carbonyl group to avoid electrostatic repulsion. The location of the chlorine atom suggests the presence of the attractive interaction between the amide NH proton (H2) and Cl2 (Cl2–H2 is 2.51(2) Å). The coplanarity between the amide plane and two aromatic rings is indicated where the torsion angles are

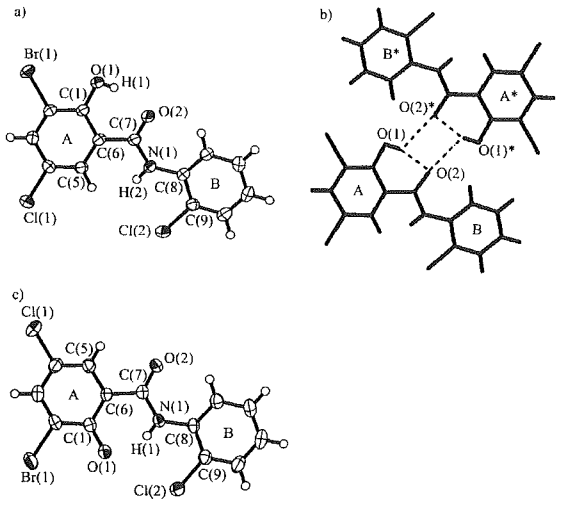


Fig. 1. ORTEP drawing (a) and packing structure (b) of **BCNCPB–OH** and ORTEP drawing of anion part of **BCNCPB–O–NEt$_4$** (c).

160.0(3)° (C5–C6–C7–O2) and 176.9(3)° (C7–N1–C8–C9). The presence of an intermolecular OH···O=C hydrogen bond is suggested by the short distance between the phenolic hydrogen atom (H1) and amide carbonyl oxygen atom (O2*) of the neighboring molecule (2.50(3) Å) (Fig. 1b). No significant intermolecular interaction around the amide NH exists.

The crystal structure of the deprotonated form (**BCNCPB–O–NEt$_4$**) is shown in Fig. 1c. A different hydrogen bonding mode from that in **BCNCPB–OH** was found. The short distances between the phenoxy oxygen (O1) and the amide proton (H1) (1.87(2) Å) and between O1 and the amide nitrogen (N1) (2.583(2) Å) suggest the presence of an intramolecular NH···O(oxyanion) hydrogen bond. The relative orientation of chlorine at the 2′-position in Ar$_B$ (Cl2) toward the amide NH is similar to that in **BCNCPB–OH**. The coplanarity of **BCNCPB–O–NEt$_4$** is higher than in **BCNCPB–OH**. The torsion angle between Ar$_A$ and amide plane (C5–C6–C7–O2) is −1.2(3)°, and that between the amide plane and Ar$_B$ (C7–N1–C8–C9) is −175.6(2)°. The C1–O1 bond length in **BCNCPB–O–NEt$_4$** (1.282(3) Å) is shorter than that in **BCNCPB–OH** (1.340(3) Å) due to an increase in the double bond character of the C1–O1 bond caused by the delocalization of the negative charge of the phenoxy anion to the aryl ring.

The most significant structural change between **BCNCPB–OH** and **BCNCPB–O–NEt$_4$** is a ca. 180 degree rotation about the C6–C7 bond.

The presence of hydrogen bonds in the solid state was confirmed by IR measurements in a Nujol mull (Fig. 2). In the protonated form, **BCNCPB–OH**, an amide NH stretching band was observed at 3416 cm$^{-1}$, which is slightly lower than non-hydrogen-bonded $\nu$(NH) ($\nu$(NH) of salicylanilide in dilute solution[20] is 3456 cm$^{-1}$) and comparable to NH···Cl hydrogen-bonded $\nu$(NH).[26,27] The orientation of Cl toward the carbonyl C=O and the amide NH is controlled by not only the electrostatic repulsion between the carbonyl oxygen and Cl but also the NH···Cl hydrogen bond. In **BCNCPB–O–NEt$_4$**, it is

Table 1. Selected Short Contacts, Bond Distance, and Torsion Angles of **BCNCPB–OH** and **BCNCPB–O–NEt$_4$**

| **BCNCPB–OH** | | **BCNCPB–O–NEt$_4$** | |
|---|---|---|---|
| | Short contacts/Å | | |
| H(2)···Cl(2) | 2.51(2) | H(1)···Cl(2) | 2.54(2) |
| H(1)···O(2) | 1.91(3) | H(1)···O(1) | 1.87(2) |
| O(1)···O(2) | 2.606(3) | O(1)···N(1) | 2.583(2) |
| H(1)···O(2)* | 2.50(3) | | |
| O(1)···O(2)* | 2.921(3) | | |
| | Bond lengths/Å | | |
| C(1)–O(1) | 1.340(3) | C(1)–O(1) | 1.282(3) |
| O(2)–C(7) | 1.223(4) | O(2)–C(7) | 1.239(3) |
| C(6)–C(7) | 1.498(4) | C(6)–C(7) | 1.484(3) |
| N(1)–C(7) | 1.353(4) | N(1)–C(7) | 1.360(3) |
| N(1)–C(8) | 1.402(4) | N(1)–C(8) | 1.400(3) |
| O(1)–H(1) | 0.74(3) | N(1)–H(1) | 0.80(2) |
| N(1)–H(2) | 0.87(3) | | |
| | Torsion angles/° | | |
| O(2)–C(7)–C(6)–C(5) | −160.0(3) | O(2)–C(7)–C(6)–C(5) | −1.2(3) |
| C(7)–N(1)–C(8)–C(9) | 176.9(3) | C(7)–N(1)–C(8)–C(9) | −175.6(2) |

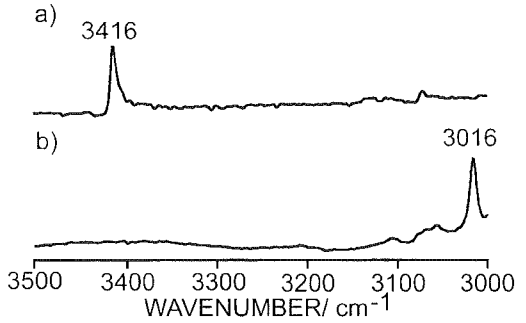


Fig. 2. IR spectra in a Nujol mull of **BCNCPB–OH** (a) and **BCNCPB–O–NEt$_4$** (b).

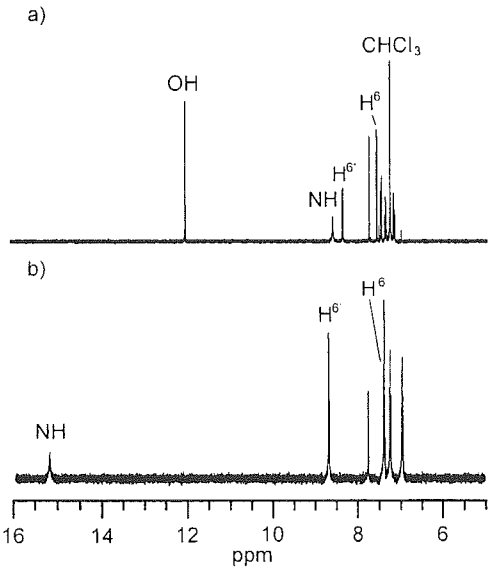


Fig. 3. $^1$H NMR spectra of **BCNCPB–OH** in $CDCl_3$ (a) and **BCNCPB–O–NEt$_4$** in $CD_3CN$ (b).

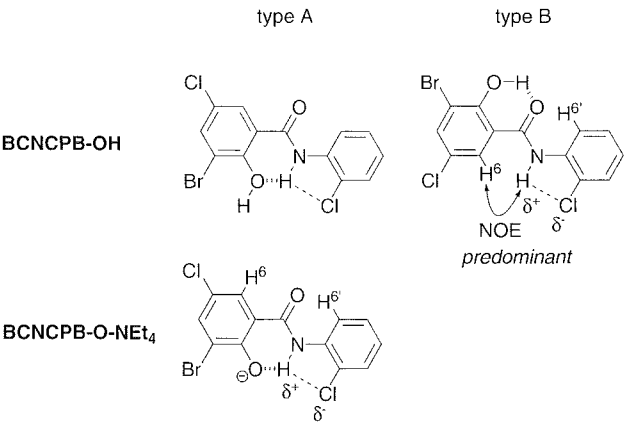


Chart 4. Solution structures of **BCNCPB–OH** and **BCNCPB–O–NEt$_4$**.

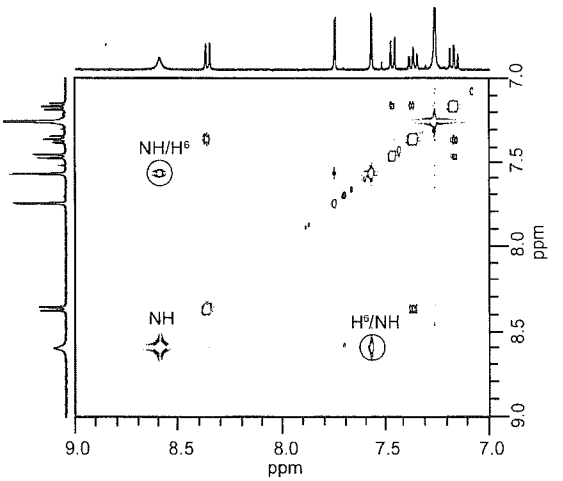


Fig. 4. NOESY spectrum of **BCNCPB–OH** in $CDCl_3$.

thought that the location of Cl2 is controlled by the same interactions. **BCNCPB–O–NEt$_4$** has an amide NH band at 3016 cm$^{-1}$, which is a very low frequency for $\nu$(NH) even if the NH proton forms a hydrogen bond, (NH···O(H)[28] 3390 cm$^{-1}$, NH···O(Ac)[29] approximately 3400 cm$^{-1}$, NH···O(carboxylate)[28] 3024 cm$^{-1}$, NH···O(phosphate)[30] 3226 cm$^{-1}$, etc.) and shows that the NH···O(oxyanion) hydrogen bond fomed in **BCNCPB–O–NEt$_4$** is very strong. The $\nu$(NH) shift in **BCNCPB–O–NEt$_4$** is comparable to that in the sodium salt of 3,5-dibromosalicylanilide,[20] which appears at 3000–2900 cm$^{-1}$.

**Solution Structures of BCNCPB–OH and BCNCPB–O–NEt$_4$.** Figure 3a shows the $^1$H NMR spectrum of **BCNCPB–OH** in $CDCl_3$. A phenolic OH signal was observed at 12.0 ppm, which is shifted to a very low field compared to non-hydrogen bonded phenolic OH (4–6 ppm), indicating the formation of a OH···O=C hydrogen bond (type B in Chart 4) similar to the solid state. An amide NH signal was observed at 8.6 ppm, which is slightly downfield compared to $\delta$(NH) in non-hydrogen bonded benzamide (6–8 ppm), showing that the weak NH···Cl hydrogen bond established in the solid state is maintained in solution. A NOE correlation between the NH and the 6-positioned aryl proton (H$^6$ at 7.6 ppm) was observed, but not between the NH and 6′-positioned aryl proton (H$^{6'}$ at 8.4 ppm) in the NOESY spectrum (Fig. 4). These results also support the type B conformation. On the other hand, a minor conformer in addition to type B was established in the IR results because of its higher time resolution than $^1$H NMR. **BCNCPB–OH** gives NH stretching bands at 3425 and 3357 cm$^{-1}$ (Fig. 5a). The ratio of each of the conformers was estimated to be about 90 and 10%, respectively, from the ratio of the area of the bands. The predominant band is assigned to the type B conformer (3416 cm$^{-1}$ in the solid state). The NH band at 3357 cm$^{-1}$ is assigned to the NH···O hydrogen bonded conformer (type A).[18,29] The band at high frequency, 3483 cm$^{-1}$, is assigned to $\nu$(OH) in the type A conformation.[20] The OH band in the type B conformation was not observed in the spectrum because of line broadning.[20]

In the $^1$H NMR spectrum of **BCNCPB–O–NEt$_4$** (Fig. 3b), an amide NH signal was observed at 15.2 ppm, which is downfield compared to the non-hydrogen bonded NH, indicating the formation of a strong NH···O(oxyanion) hydrogen bond (type A) similar to the solid state. The NH shows no NOE correlation with other protons in the NOESY spectrum (data not shown). It also supports the type A conformation. The IR results (Fig. 5b), where an NH band was observed at 3015

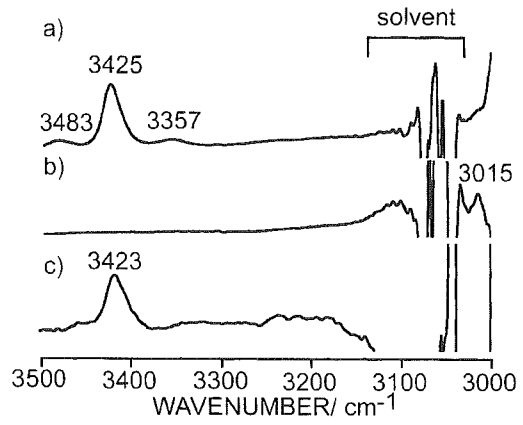


Fig. 5. IR spectra of 5 mM $CH_2Cl_2$ solution of **BCNCPB–OH** (a), **BCNCPB–O–NEt$_4$** (b), and BH3I-2′ (c).

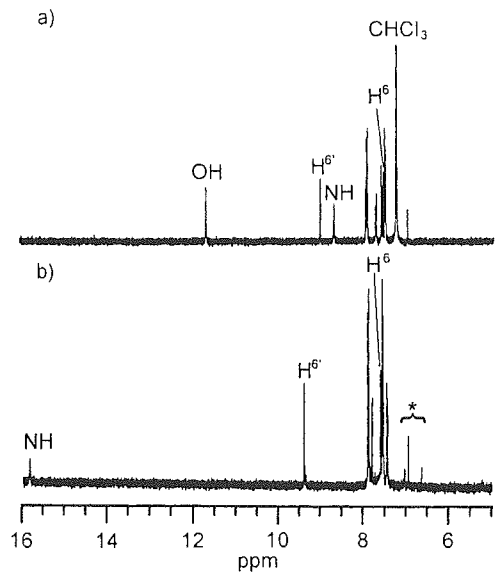


Fig. 6. $^1$H NMR spectra of BH3I-2′ in $CDCl_3$ (a) and deprotonated BH3I-2′ in $CD_3CN$ (b).

cm$^{-1}$, also show strong NH···O(oxyanion) hydrogen bonding.

**Solution Structures of BH3I-2′.** Figure 6a shows the $^1$H NMR spectrum of BH3I-2′. Phenolic OH and amide NH signals were observed at 11.7 and 8.7 ppm, respectively. These similar chemical shifts to **BCNCPB–OH** show that BH3I-2′ has similar hydrogen bonds (Chart 5). An observed NOE correlation between the NH and the 6-positioned aryl proton ($H^6$ at 7.5 ppm) supports the type B conformation (Fig. 7). However, BH3I-2′ gives one NH band at 3423 cm$^{-1}$ in the IR spectrum that is different from **BCNCPB–OH** (Fig. 5c). This is because iodine acts as a weaker hydrogen bonding accepter (OH···I) compared to bromine due to a smaller electronegativity. BH3I-2, which has bromine, probably has a minor conformer similar to **BCNCPB–OH**.

In the $^1$H NMR spectrum of deprotonated BH3I-2′ (Fig. 6b), an amide NH signal was observed at 15.8 ppm, which is extremely downfield, similar to **BCNCPB–O–NEt$_4$**. This indicates NH···O(oxyanion) hydrogen bonding (type A). The type A conformation is also supported by the disappearance of the

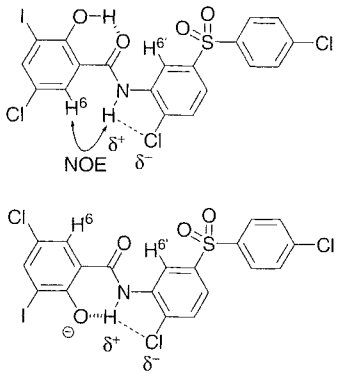


Chart 5. Solution structures of protonated and deprotonated forms of BH3I-2′.

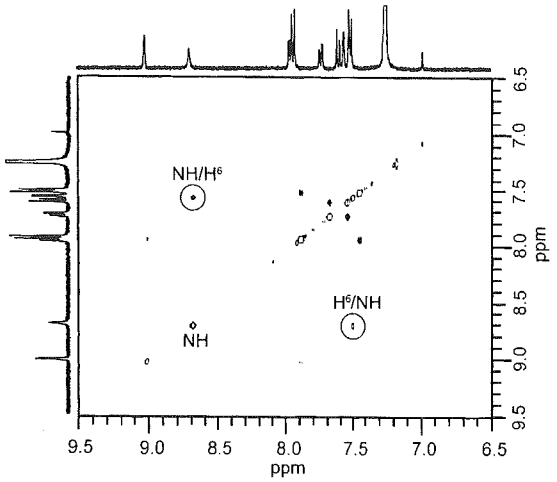


Fig. 7. NOESY spectrum of protonated BH3I-2′ in $CDCl_3$.

NOE correlation regarding NH.

Protonated and deprotonated BH3I-2′ form similar hydrogen bonds to the predominant conformations of **BCNCPB–OH** and **BCNCPB–O–NEt$_4$**, respectively. BH3I-2 probably prefers similar conformations.

**p$K_a$ of BCNCPB–OH in an Aqueous Micellar Solution.** The pH titration of **BCNCPB–OH** was performed in an aqueous micellar solution. Under these conditions, **BCNCPB–OH** is incorporated into the hydrophobic layer where the hydrogen bonds are supported. These conditions also realize a hydrophobic cleft formed in Bcl-xL where BH3I-2 binds.[1] The titration method using an aqueous micellar solution is adequate to mimic the hydrophobic environments inside of protein.[23,24] Because protons can move inside and outside of micelles freely, the p$K_a$ value of **BCNCPB–OH** is evaluated by pH measurements in the aqueous layer. **BCNCPB–OH** exists inside micelles due to its poor solubility in water during the titration. The p$K_a$ value of **BCNCPB–OH** obtained from the titration was 5.1, which is very low compared with phenol (9.9 in water[31]). In addition to the electron-withdrawing effect of Cl, Br, and the aryl *N*-substituent ($Ar_B$), the existence of amide NH, which forms an intramolecular NH···O(oxyanion) hydrogen bond in the deprotonated form, lowers the p$K_a$ value.[19,23,28] The p$K_a$ value of BH3I-2 should be equal to or slightly less than 5.1 because an additional electron withdrawing substitu-

ent, the 4-chlorophenylsulfonyl group on the *N*-2-chlorophenyl group, of BH3I-2 has little effect on its acidity.[11]

**Proposed Binding Structure of BH3I-2.** The structure of the BH3I-2/Bcl-xL complex has been computationally proposed using the solution structure of the BakBH3–peptide/Bcl-xL complex.[1,21,22] This is based on the fact that the structure of Bcl-xL and the inhibitor–binding site are similar to those of the BakBH3–peptide/Bcl-xL complex. In this complex, BH3I-2 binds to a hydrophobic cleft formed by the BH1, BH2, and BH3 regions. The 3-positioned bromine interacts with the side chain of Tyr65 and the 5-positioned chlorine with the side chain of Phe61 and Phe110, etc. The presence of the interactions is demonstrated by a change in the inhibitory activity induced by the substitution of these halogen atoms. In the complex, the structure of BH3I-2 is represented in the protonated form and has an intramolecular NH···O hydrogen bond (type A). Our structural analysis of BH3I-2, however, shows that BH3I-2 forms an intramolecular OH···O=C hydrogen bond (type B) in the protonated form. It is difficult to fit BH3I-2 into the hydrophobic cleft while keeping the intramolecular OH···O=C hydrogen bond and the interactions between bromine–Tyr65, chlorine–Phe110, and chlorine–Phe61, because the chlorine on the *N*-aryl ring would be too close to the side chain of Phe61 or Ala106 under this assumption (Fig. 8b). On the other hand, it is reasonable that BH3I-2 binds in the deprotonated form in which an intramolecular NH···O(oxyanion) hydrogen bond is formed (Fig. 8a). This suggestion is supported by the p$K_a$ value of BH3I-2 of about 5.1, which indicates that BH3I-2 is deprotonated under physiological conditions (pH = 7.2).[2] It is possible that Tyr65 does not interact with bromine but forms an intermolecular OH(Tyr)···O(oxyanion) hydrogen bond.

Different from other salicylamide inhibitors noted above, BH3I-2 binds to the protein in deprotonated form. This is because the p$K_a$ value of BH3I-2 is lower than others due to strong electron-withdrawing substituents (Cl ($\sigma_{para} = 0.23$) and Br ($\sigma_{para} = 0.23$)) compared to others (F ($\sigma_{para} = 0.06$) or NHCHO ($\sigma_{para} = 0.00$)).[25]

## Conclusion

In this study, BH3I-2 models, **BCNCPB–OH** and **BCNCPB–O–NEt$_4$**, were synthesized and structurally analyzed. The presence of an intramolecular OH···O=C hydrogen bond in **BCNCPB–OH** and an intramolecular NH···O(oxyanion) hydrogen bond in **BCNCPB–O–NEt$_4$** as established by X-ray analyses and IR spectra. The $^1$H NMR and IR results of **BCNCPB–O–NEt$_4$** have revealed that the structure in the solid state is maintained in dilute solution with similar hydrogen bonds. **BCNCPB–OH** prefers a similar conformation to the solid state predominantly, but has a minor conformer having an NH···O hydrogen bond. $^1$H NMR and IR spectra show that the protonated and deprotonated BH3I-2′ form intramolecular hydrogen bonds in the same manner as the corresponding models except for no evidence of the minor conformers in the protonated form. The deprotonation of BH3I-2 in the BH3I-2/Bcl-xL complex is suggested by the low p$K_a$ value of **BCNCPB–OH**. It is also supported by the possible OH-(Tyr)···O(oxyanion) hydrogen bond formation between the OH group of Tyr65 and the phenoxy oxygen atom of BH3I-2.

## Experimental

**Materials.** BH3I-2′ was purchased from CALBIOCHEM. Other reagents were purchased from Nacalai Tesque or Tokyo Chemical Industry and used without further purification. All organic solvents were dried over $CaH_2$ and distilled under an Ar atmosphere before use.

**Synthesis. 3-Bromo-5-chloro-2-hydroxybenzoic Acid (1):** This compound was prepared using a modified method reported in the literature.[32]

To a solution of 3-bromo-5-chloro-2-hydroxybenzaldehyde (278 mg, 1.3 mmol) in dioxane (15 mL) were added $NaH_2PO_4$ (800 mg, 5.1 mmol) in water (5 mL) and sulfamic acid (186 mg, 1.92 mmol). The reaction mixture was cooled to 7 °C and then NaClO2 (186 mg, 1.7 mmol) in water (0.7 mL) was added gradually while keeping the temperature below 10 °C. The reaction mixture was stirred for 30 min below 10 °C. Sodium sulfite (195 mg, 1.5 mmol) was added with stirring for 15 min below 10 °C. Hydrochloric acid was added until a pH of 1 was obtained. Volatile materials were evaporated, and the resulting solution was cooled to deposit a white precipitate, which was collected by filtration and washed with water (309 mg, 94%).

Anal. Found: C, 33.37; H, 1.63%. Calcd for $C_7H_4BrClO_3$: C, 33.43; H, 1.60%. Mp: 238–239 °C. $^1$H NMR (DMSO-$d_6$; TMS) $\delta$ 7.91 (1H, m, Ar–H), 7.74 (1H, m, Ar–H). $^{13}$C NMR (DMSO-$d_6$): $\delta$ 170.3, 156.7, 137.3, 128.7, 122.8, 115.3, 111.3. ESI-MS:

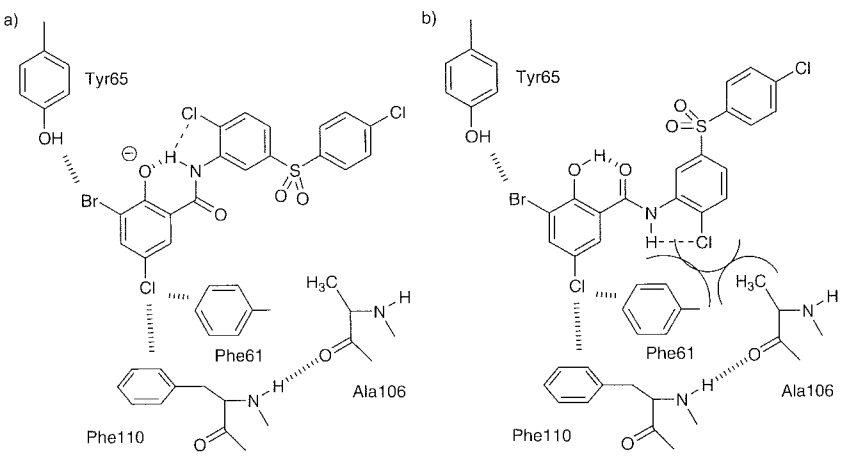


Fig. 8. Proposed binding structure in type A conformation (a) and type B conformation (b).

$(M - H^+)^-$, 249.1 (calcd for $M - H^+$; 248.90).

**2-Acetoxy-3-bromo-5-chlorobenzoic Acid (2):** 3-Bromo-5-chloro-2-hydroxybenzoic acid (519.3 mg, 2.1 mmol) was dissolved in 10 mL of THF. To the solution was added acetyl chloride (0.15 mL, 2.1 mmol), followed by triethylamine (0.3 mL, 2.2 mmol). The reaction mixture was stirred overnight, and the white precipitate was then filtered out. The filtrate was concentrated under reduced pressure. The resultant white powder was used without further purification (555 mg, 92%).

Mp: 153–155 °C. $^1$H NMR ($CDCl_3$; TMS) $\delta$ 8.01 (1H, d, $J$ = 2.4 Hz, Ar–H), 7.83 (1H, d, $J$ = 2.4 Hz, Ar–H), 2.38 (3H, s, $CH_3$). $^{13}$C NMR ($CDCl_3$): $\delta$ 168.0, 167.6, 147.3, 137.5, 132.1, 131.2, 125.1, 119.5, 20.7. ESI-MS: $(M - H^+)^-$, 290.9 (calcd for $M - H^+$; 290.91).

**2-(2-Chlorophenylcarbamoyl)-6-bromo-4-chlorophenyl Acetate (3):** 2-Acetoxy-3-bromo-5-chlorobenzoic acid (319 mg, 1.1 mmol) and triethylamine (0.20 mL, 1.4 mmol) were dissolved in 40 mL of THF. The solution was cooled to −20 °C. To the solution was added isobutyl chloroformate (IBCF) (0.18 mL, 1.4 mmol) gradually, keeping the temperature under −15 °C. After stirring for 5 min, *o*-chloroaniline (0.15 mL, 1.4 mmol) in THF (4 mL) was dropped into the reaction mixture. The reaction mixture was stirred for 1 h at −15 °C, and then 2 days at room temperature. The solvent was removed, and the residue was extracted with ethyl acetate and washed with 2% HCl aq., 4% $NaHCO_3$ aq., and sat. NaCl aq., and then dried over anhydrous sodium sulfate. The removal of the solvent gave a brown oily residue. The reprecipitation from diethyl ether/hexane gave a white powder. Recrystallization from ethyl acetate/hexane gave colorless needles (169 mg, 62%).

Mp: 128–129 °C. $^1$H NMR ($CDCl_3$; TMS) $\delta$ 8.54 (1H, s, NH), 8.49 (1H, d, $J$ = 7.6 Hz, $Ar_B$–H), 7.85 (1H, d, $J$ = 2.4 Hz, $Ar_A$–H), 7.76 (1H, d, $J$ = 2.4 Hz, $Ar_A$–H: protons on phenolic moiety), 7.41 (1H, dd, $J$ = 8.4, 1.6 Hz, $Ar_B$–H: protons on *N*-aryl group), 7.33 (1H, t, $J$ = 8.4 Hz, $Ar_B$–H), 7.09 (1H, dt, $J$ = 7.6, 1.6 Hz, $Ar_B$–H), 2.41 (3H, s, $CH_3$). $^{13}$C NMR ($CDCl_3$) $\delta$ 167.6, 161.1, 144.3, 135.6, 134.1, 132.8, 131.2, 129.4, 129.1, 127.9, 125.4, 122.9, 121.8, 118.9, 21.0. ESI-MS: $(M - H^+)^-$, 399.7 (calcd for $M - H^+$; 399.91).

**3-Bromo-5-chloro-*N*-(2-chlorophenyl)-2-hydroxybenzamide (BCNCPB–OH):** 2-(2-chlorophenylcarbamoyl)-6-bromo-4-chlorophenyl acetate (169 mg, 0.42 mmol) was dissolved in a mixture of MeOH (2 mL) and 1 M NaOH aq. (1 mL). The solution was stirred for two days and acidified by 2% HCl aq. The precipitated white powder was collected by filtration and recrystallized from THF/hexane. Colorless needles were obtained (34 mg, 23%).

Anal. Found: C, 43.23; H, 2.20; N, 3.83%. Calcd for $C_{13}H_8BrCl_2NO_2$: C, 43.25; H, 2.23; N, 3.88%. Mp: 157–160 °C. $^1$H NMR ($CDCl_3$; TMS) $\delta$ 12.02 (1H, s, OH), 8.59 (1H, s, NH), 8.36 (1H, dd, $J$ = 8.4, 1.6 Hz, $Ar_B$–H), 7.74 (1H, d, $J$ = 2.4 Hz, $Ar_A$–H), 7.56 (1H, d, $J$ = 2.4 Hz, $Ar_A$–H), 7.46 (1H, dd, $J$ = 7.6, 1.6 Hz, $Ar_B$–H), 7.36 (1H, dt, $J$ = 8.4, 1.6 Hz, $Ar_B$–H), 7.16 (1H, dt, $J$ = 7.6, 1.6 Hz, $Ar_B$–H). $^{13}$C NMR ($CDCl_3$) $\delta$ 165.9, 156.4, 137.2, 133.0, 129.2, 127.8, 126.0, 124.9, 124.2, 121.1, 122.4, 116.4, 113.4. ESI-MS: $(M - H^+)^-$, 358.1 (calcd for $M - H^+$; 357.90).

**Tetraethylammonium 2-Bromo-4-chloro-6-[*N*-(2-chlorophenyl)carbamoyl]phenolate (BCNCPB–O–NEt$_4$):** 3-Bromo-5-chloro-*N*-(2-chlorophenyl)-2-hydroxybenzamide (44.9 mg, 0.12 mmol) was dissolved in 8 mL of methanol. To the solution was added a 25% tetraethylammonium hydroxide aqueous solution (0.09 mL). The solution was stirred for 1 h, and solvents were removed under reduced pressure. The residue was washed with 10 mL of diethyl ether twice. The resultant powder was recrystallized from THF/diethyl ether to give **BCNCPB–O–NEt$_4$** as hygroscopic yellow crystals.

Anal. Found: C, 50.45; H, 5.52; N, 5.56%. Calcd for $C_{21}H_{27}BrCl_2N_2O_2 + (H_2O)_{0.5}$: C, 50.52; H, 5.65; N, 5.61%. Mp: 108–111 °C. $^1$H NMR ($CD_3CN$; TMS) $\delta$ 15.22 (1H, s, NH), 8.70 (1H, dd, $J$ = 8.0, 1.6 Hz, $Ar_B$–H), 7.77 (1H, dd, $J$ = 3.2, 0.8 Hz, $Ar_A$–H), 7.40 (1H, dd, $J$ = 7.6, 1.6 Hz, $Ar_B$–H), 7.39 (1H, d, $J$ = 3.2 Hz, $Ar_A$–H), 7.25 (1H, tt, $J$ = 8.0, 1.6 Hz, $Ar_B$–H), 6.96 (1H, tt, $J$ = 7.6, 1.6 Hz, $Ar_B$–H), 3.14 (8H, q, $J$ = 7.6 Hz, 4 × $CH_2CH_3$), 1.19 (12H, tt, $J$ = 7.6, 2.0 Hz, 4 × $CH_2CH_3$). $^{13}$C NMR ($CD_3CN$) $\delta$ 167.5, 167.2, 139.2, 134.7, 130.1, 129.4, 128.0, 123.8, 123.7, 123.1, 120.1, 119.1, 112.5, 53.1, 7.6.

**Deprotonation of BH3I-2′.** BH3I-2′ (1.5 mg, 2.8 μmol) was dissolved in 2 mL of THF. To the solution was added one drop of 25% tetraethylammonium hydroxide aqueous solution. The solution was then concentrated in vacuo. The residue was washed with 2 mL of diethyl ether and dried in vacuo.

**$^1$H NMR Results of BH3I-2′ and Deprotonated BH3I-2′.** BH3I-2′: $^1$H NMR ($CDCl_3$; TMS) $\delta$ 11.70 (1H, s, OH), 9.01 (1H, d, $J$ = 2.0 Hz, $Ar_B$–H), 8.69 (1H, s, NH), 7.96 (1H, d, $J$ = 2.4 Hz, $Ar_A$–H), 7.93 (2H, d, $J$ = 8.8 Hz, $Ar_C$–H: protons on *p*-chlorophenyl group), 7.73 (1H, dd, $J$ = 8.8, 2.0 Hz, $Ar_B$–H), 7.60 (1H, d, $J$ = 8.8 Hz, $Ar_B$–H), 7.56 (1H, d, $J$ = 2.4 Hz, $Ar_A$–H), 7.52 (2H, d, $J$ = 8.8 Hz, $Ar_C$–H).

Deprotonated BH3I-2′: $^1$H NMR ($CD_3CN$; TMS) $\delta$ 15.85 (1H, s, NH), 9.41 (1H, d, $J$ = 2.4 Hz, $Ar_B$–H), 7.90 (2H, d, $J$ = 9.2 Hz, $Ar_C$–H), 7.82 (1H, d, $J$ = 2.8 Hz, $Ar_A$–H), 7.63 (1H, d, $J$ = 2.8 Hz, $Ar_A$–H), 7.58 (1H, d, $J$ = 8.4 Hz, $Ar_B$–H), 7.57 (2H, d, $J$ = 9.2 Hz, $Ar_C$–H), 7.46 (1H, dd, $J$ = 8.4, 2.4 Hz, $Ar_B$–H), 3.14 (8H, q, $J$ = 7.6 Hz, 4 × $CH_2CH_3$), 1.19 (12H, tt, $J$ = 7.6, 2.0 Hz, 4 × $CH_2CH_3$).

**Physical Measurements.** $^1$H NMR spectra in a $CDCl_3$ or $CD_3CN$ solution were recorded on a JEOL GSX 400 spectrometer and a JEOL JNM EX 270 at 30 °C. NOESY spectra were recorded on a Varian UNITYplus 600 MHz spectrometer at 30 °C. Tetramethylsilane was used as a standard (0 ppm). $^{13}$C NMR spectra in $CDCl_3$, $CD_3CN$, and DMSO-$d_6$ were recorded on a JEOL JNM EX 270 and Varian UNITYplus 600 MHz at 30 °C. Signals of the solvent were used as a standard {77.0 ppm ($CDCl_3$), 118.2 ppm ($CD_3CN$), and 39.7 ppm (DMSO-$d_6$)}. ESI-MS measurements were performed on a Finnigan MAT LCQ ion trap mass spectrometer in a methanol solution. IR spectra were recorded on a Jasco FT/IR 8300 spectrometer. Samples were prepared as Nujol mulls and in $CH_2Cl_2$ solution (1 and 5 mM).

**pH Titration.** The pH of a 10 mM **BCNCPB–OH** solution was determined using a Metrohm 716 DMS titrino, which is combined with a Metrohm 728 stirrer and a saturated calomel LL micro pH glass electrode. The saturated calomel micro glass electrode was calibrated with a 0.05 M $KHC_6H_4(COO)_2$ buffer (pH = 4.01), and a 0.025 M $KH_2PO_4$–$Na_2HPO_4$ buffer (pH = 6.86) at 30 °C. **BCNCPB–OH** was dissolved in a small amount of THF, and to this solution was added Triton X-100. The solution was concentrated to remove THF. The obtained residue was diluted with degassed water to give a micellar solution. The final concentration was a 10% Triton X-100 aqueous solution containing 10 mM of **BCNCPB–OH**. The solution was titrated with 0.1 M NaOH aq. at 30 °C. The $pK_a$ value was estimated by the following equation:[23,24] $pK_a = pH - \log[Na^+] + \log\{[phenol]_0 - [Na^+]\}$.

**X-ray Structure Determination.** Each single crystal of **BCNCPB–OH** and **BCNCPB–O–NEt$_4$** was mounted in a loop

with Nujol. The X-ray data were collected at 200 K on a Rigaku Raxis-RAPID Imaging Plate diffractometer with graphite monochromated Mo K$\alpha$ ($\lambda = 0.71075$ Å). The basic crystallographic parameters are listed in Table S1 (See Supporting Information). A symmetry-related absorption correction using the program ABSCOR[33] was applied, which resulted in transmission factors ranging from 0.43 to 0.49 for **BCNCPB–OH** and 0.42 to 0.53 for **BCNCPB–O–NEt$_4$**. The structure was solved by the direct method (SHELXS-97[34] for **BCNCPB–OH** and SIR92[35] for **BCNCPB–O–NEt$_4$**) and expanded using Fourier techniques using *teXsan* crystallographic software[36] and SHELXL-97.[37] Non-hydrogen atoms were refined anisotropically. The positions of OH and NH were refined using fixed thermal parameters, and the other hydrogen atoms were placed at calculated positions.

**Crystal Data.** **BCNCPB–OH:** $C_{13}H_8BrCl_2NO_2$, $M = 361.02$, orthorhombic, $a = 23.15(2)$, $b = 15.73(2)$, $c = 7.126(7)$ Å, $U = 2594(10)$ Å$^3$, $T = 200$ K, space group *Pccn* (no. 56), $Z = 8$, $\mu = 35.84$ cm$^{-1}$, 22578 reflections measured, 2836 unique ($R_{int} = 0.096$), $R_1 = 0.036$ ($I > 2\sigma$), $wR_2 = 0.070$ (all data).

**BCNCPB–O–NEt$_4$:** $C_{21}H_{27}BrCl_2N_2O_2$, $M = 490.27$, orthorhombic, $a = 7.307(4)$, $b = 16.18(1)$, $c = 18.99(1)$ Å, $U = 2245(8)$ Å$^3$, $T = 200$ K, space group $P2_12_12_1$ (no. 19), $Z = 4$, $\mu = 20.93$ cm$^{-1}$, 21267 reflections measured, 2935 unique ($R_{int} = 0.045$), $R_1 = 0.028$ ($I > 2\sigma$), $wR_2 = 0.048$ (all data).

One of the authors (DK) expresses his special thanks to the center of excellence (21COE) program "Creation of Integrated EcoChemistry of Osaka University".

## References

1 A. A. Lugovskoy, A. I. Degterev, A. F. Fahmy, P. Zhou, J. D. Gross, J. Yuan, and G. Wagner, *J. Am. Chem. Soc.*, **124**, 1234 (2002).

2 A. Degterev, A. Lugovskoy, M. Cardone, B. Mulley, G. Wagner, T. Mitchison, and J. Yuan, *Nat. Cell Biol.*, **3**, 173 (2001).

3 X. Gao, X. Wen, L. Esser, B. Quinn, L. Yu, C.-A. Yu, and D. Xia, *Biochemistry*, **42**, 9067 (2003).

4 H. Miyoshi, N. Tokutake, Y. Imaeda, T. Akagi, and H. Iwamura, *Biochim. Biophys. Acta*, **1229**, 149 (1995).

5 N. Tokutake, H. Miyoshi, T. Satoh, T. Hatano, and H. Iwamura, *Biochim. Biophys. Acta*, **1185**, 271 (1994).

6 D. L. Selwood, D. J. Livingstone, J. C. W. Comley, A. B. O'Dowd, A. T. Hudson, P. Jackson, K. S. Jandu, V. S. Rose, and J. N. Stables, *J. Med. Chem.*, **33**, 136 (1990).

7 Z. Wawrzak, T. Sandalova, J. J. Steffens, G. S. Basarab, T. Lundqvist, Y. Lindqvist, and D. B. Jordan, *Proteins: Struct., Funct., Genet.*, **35**, 425 (1999).

8 C. N. Hodge and J. Pierce, *Bioorg. Med. Chem. Lett.*, **3**, 1605 (1993).

9 R. L. Williamson and R. L. Metcalf, *Science*, **158**, 1694 (1967).

10 B. T. Storey, D. F. Wilson, A. Bracey, S. L. Rosen, and S. Stephenson, *FEBS Lett.*, **49**, 338 (1975).

11 H. Terada, S. Goto, K. Yamamoto, I. Takeuchi, Y. Hamada, and K. Miyake, *Biochim. Biophys. Acta*, **936**, 504 (1988).

12 M. J. Macielag, J. P. Demers, S. A. Fraga-Spano, D. J. Hlasta, S. G. Johnson, R. M. Kanojia, R. K. Russell, Z. Sui, M. A. Weidner-Wells, H. Werblood, B. D. Foleno, R. M. Goldschmidt, M. J. Loeloff, G. C. Webb, and J. F. Barrett, *J. Med. Chem.*, **41**, 2939 (1998).

13 D. J. Hlasta, J. P. Demers, B. D. Foleno, S. A. Fraga-Spano, J. Guan, J. J. Hilliard, M. J. Macielag, K. A. Ohemeng, C. M. Sheppard, Z. Sui, G. C. Webb, M. A. Weidner-Wells, H. Werblood, and J. F. Barrett, *Bioorg. Med. Chem. Lett.*, **8**, 1923 (1998).

14 H. Kim, L. Esser, M. B. Hossain, D. Xia, C.-A. Yu, J. Rizo, D. van der Helm, and J. Deisenhofer, *J. Am. Chem. Soc.*, **121**, 4902 (1999).

15 K. M. Kim, C. D. Giedt, G. Basañez, J. W. O'Neil, J. J. Hill, Y.-H. Han, S.-P. Tzung, J. Zimmerberg, D. M. Hockenbery, and K. Y. J. Zhang, *Biochemistry*, **40**, 4911 (2001).

16 S.-P. Tzung, K. M. Kim, G. Basañez, C. D. Giedt, J. Simon, J. Zimmerberg, K. Y. J. Zhang, and D. M. Hockenbery, *Nat. Cell Biol.*, **3**, 183 (2001).

17 F. Mu, E. Hamel, D. J. Lee, D. E. Pryor, and M. Cushman, *J. Med. Chem.*, **46**, 1670 (2003).

18 H. Suezawa, M. Hirota, T. Yuzuki, Y. Hamada, I. Takeuchi, and M. Sugiura, *Bull. Chem. Soc. Jpn.*, **73**, 2335 (2000).

19 W. L. Mock and D. C. Y. Chua, *J. Chem. Soc., Perkin Trans. 2*, **1995**, 2069.

20 D. Welti, *Spectrochim. Acta*, **22**, 281 (1966).

21 M. Sattler, H. Liang, D. Nettesheim, R. P. Meadows, J. E. Harlan, M. Eberstadt, H. S. Yoon, S. B. Shuker, B. S. Chang, A. J. Minn, C. B. Thompson, and S. W. Fesik, *Science*, **275**, 983 (1997).

22 A. Fahmy and G. Wagner, *J. Am. Chem. Soc.*, **124**, 1241 (2002).

23 N. Ueyama, M. Inohara, A. Onoda, T. Ueno, T. Okamura, and A. Nakamura, *Inorg. Chem.*, **38**, 4028 (1999).

24 A. Onoda, Y. Yamada, J. Takeda, Y. Nakayama, T. Okamura, M. Doi, H. Yamamoto, and N. Ueyama, *Bull. Chem. Soc. Jpn.*, **77**, 321 (2004).

25 C. Hansch, A. Leo, and R. W. Taft, *Chem. Rev.*, **91**, 165 (1991).

26 Y. Mido and T. Okuno, *J. Mol. Struct.*, **82**, 29 (1982).

27 Y. Mido, M. Sakoda, and K. Fujiwara, *J. Mol. Struct.*, **350**, 205 (1995).

28 A. Onoda, T. Okamura, H. Yamamoto, and N. Ueyama, *Acta Crystallogr.*, **E59**, o1202 (2003).

29 H. Endo, M. Hirota, Y. Ito, I. Takeuchi, and Y. Hamada, *Bull. Chem. Soc. Jpn.*, **55**, 1564 (1982).

30 A. Onoda, Y. Yamada, T. Okamura, M. Doi, H. Yamamoto, and N. Ueyama, *J. Am. Chem. Soc.*, **124**, 1052 (2002).

31 A. I. Biggs and R. A. Robinson, *J. Chem. Soc.*, **1961**, 388.

32 M. A. Weidner-Wells and S. A. Fraga-Spano, *Synth. Commun.*, **26**, 2775 (1996).

33 T. Higashi, "Program for Absorption Correction," Rigaku Corporation, Tokyo, Japan (1995).

34 SHELXS-97: G. M. Sheldrick, "Program for the Refinement of Crystal," University of Göttingen, Germany (1997).

35 A. Altomare, M. C. Burla, M. Camalli, M. Cascarano, C. Giacovazzo, A. Guagliardi, and G. Polidori, *J. Appl. Crystallogr.*, **27**, 435 (1994).

36 teXsan: "Crystal Structure Analysis Package," Molecular Structure Corporation (1985, 1999).

37 SHELXL-97: G. M. Sheldrick, "Program for the Refinement of Crystal," University of Göttingen, Germany (1997).

*Accelerated Publication*

THE JOURNAL OF BIOLOGICAL CHEMISTRY
Vol. 280, No. 2, Issue of January 14, pp. 857–860, 2005


# Nuclear Translocation of Caspase-3 Is Dependent on Its Proteolytic Activation and Recognition of a Substrate-like Protein(s)*[S]

Received for publication, November 19, 2004
Published, JBC Papers in Press, November 29, 2004,
DOI 10.1074/jbc.C400538200

**Shinji Kamada‡§¶‖, Ushio Kikkawa§, Yoshihide Tsujimoto¶, and Tony Hunter‡****

*From the ‡Molecular and Cell Biology Laboratory, The Salk Institute, La Jolla, California 92037, the §Biosignal Research Center, Kobe University, 1-1 Rokkodai-cho, Nada-ku, Kobe, Hyogo 657-8501, Japan, and the ¶Laboratory of Molecular Genetics, Department of Post-Genomics and Diseases, Osaka University Medical School and Graduate School of Medicine, 2-2 Yamadaoka, Suita, Osaka 565–0871, Japan*

**Caspase-3 is thought to play an important role(s) in the nuclear morphological changes that occur in apoptotic cells and many nuclear substrates for caspase-3 have been identified despite the cytoplasmic localization of procaspase-3. Therefore, whether activated caspase-3 is localized in the nuclei and how active caspase-3 has access to its nuclear targets are important and unresolved questions. Here we confirmed nuclear localizations for both caspase-3-p17 and caspase-3-p12 subunits of active caspase in apoptotic cells using subcellular fractionation analysis. We also prepared polyclonal and monoclonal antibodies specific for active caspase-3 to define the subcellular localization of active caspase-3. Immunocytochemical observations using anti-active caspase-3 antibodies showed nuclear accumulation of active caspase-3 during apoptosis. In addition, caspase-3, but not caspase-7, translocated from the cytoplasm into the nucleus after induction of apoptosis. Mutations at the cleavage site between the p17 and p12 subunits and the substrate recognition site for the P3 amino acid of the DXXD substrate cleavage motif inhibited nuclear translocation of caspase-3, indicating that nuclear transport of active caspase-3 required proteolytic activation and substrate recognition. These results suggest that active caspase-3 is translocated in association with a substrate-like protein(s) from the cytoplasm into the nucleus during progression through apoptosis.**

Apoptosis is a fundamental cellular process involved in many biological phenomena, including morphogenesis and maintenance of tissue homeostasis. Apoptosis is morphologically characterized by a dramatic execution phase that includes loss of cell volume, plasma membrane blebbing, and chromatin condensation followed by packaging of the cellular contents into membrane-enclosed vesicles called apoptotic bodies. These changes reflect complex biochemical events carried out by a family of cysteine proteases called caspases (1). Caspases are divided into initiator caspases with long prodomains (caspase-8, -9, and -10) and effector caspases with short prodomains (caspase-3, -6, and -7). Initiator caspases activate effector caspases, which in turn cleave intracellular substrates, resulting in the dramatic morphological and biochemical changes characteristic of apoptosis (2–4).

Caspase-3 has been implicated as a key mediator of apoptosis in mammalian cells and is synthesized as a latent proenzyme composed of 277 amino acids (5–9). In response to various death signals, the caspase-3 proenzyme is cleaved by initiator caspases at $Asp^{28}$ and $Asp^{175}$ to generate the active large (p17) and small (p12) subunits, forming an active heterotetramer. Although the precursor form of caspase-3 is localized in the cytoplasm, caspase-3 plays essential roles in the nuclear changes in apoptotic cells (9, 10). These results suggested that some cytoplasmic substrates translocate into the nucleus after cleavage by caspase-3 leading to nuclear morphological changes. In this scenario, caspase-activated DNase (CAD)[1]/DNA fragmentation factor (DFF) 40 and apoptotic chromatin condensation inducer in the nucleus (Acinus) were identified in the cytoplasmic fraction of apoptotic cells (11–13). However, CAD/DFF40 and Acinus were suggested to be localized in the nucleus even before apoptosis induction (12–14). Furthermore, many substrates for caspase-3 have been identified in the nucleus (2–4, 15). Therefore, caspase-3 seems to translocate from the cytoplasm into the nucleus after apoptosis induction, and it was proposed that active caspase-3 is translocated into nuclei by simple diffusion after disruption of nuclear-cytoplasmic barrier (16). However, the precise molecular mechanism of nuclear translocation of active caspase-3 is still unknown.

In the present study, we have demonstrated the nuclear localization of active caspase-3 in apoptotic cells by using antibodies specific for the large and small subunits of active caspase-3. Furthermore, we have shown that the nuclear translocation of active caspase-3 required proteolytic activation and substrate recognition by using caspase-3 mutants, suggesting that the nuclear translocation of active caspase-3 is not mediated by simple diffusion but is operated by an active transport system.

## EXPERIMENTAL PROCEDURES

*Cell Culture and Apoptosis Induction*—HepG2 cells were cultured in RPMI 1640 medium with 10% fetal bovine serum (FBS). For induction of apoptosis, HepG2 cells were treated with 1 μg/ml of an agonistic anti-Fas antibody (CH-11; Kamiya Biomedical Co.) in the presence of 0.2 μg/ml actinomycin D or with 200 μg/ml etoposide. Transfection was performed using GenePORTER 2 (Gene Therapy Systems) according to the manufacturer's instructions.

* This work was supported in part by grants-in-aid for Scientific Research on Priority Areas from the Ministry of Education, Science, Sports, and Culture of Japan (to S. K.) and by Public Health Service Grants CA82863 and CA14195 from the NCI (to T. H.). The costs of publication of this article were defrayed in part by the payment of page charges. This article must therefore be hereby marked "*advertisement*" in accordance with 18 U.S.C. Section 1734 solely to indicate this fact.

[S] The on-line version of this article (available at http://www.jbc.org) contains supplemental Experimental Procedures, Results, and Fig. S1.

‖ To whom correspondence may be addressed. Tel.: 81-78-803-5965; Fax: 81-78-803-5972; E-mail: skamada@kobe-u.ac.jp.

** Frank and Else Schilling American Cancer Society Professor. To whom correspondence may be addressed: Molecular and Cell Biology Laboratory, The Salk Inst., 10010 North Torrey Pines Rd., La Jolla, CA 92037. Tel.: 858-453-4100; Fax: 858-457-4765; E-mail: hunter@salk.edu.

[1] The abbreviations used are: CAD, caspase-activated DNase; DFF, DNA fragmentation factor; GFP, green fluorescent protein; TXRD, Texas Red; PBS, phosphate-buffered saline; pAb, polyclonal antibody; PKC, protein kinase C; NPC, nuclear pore complex.

*Subcellular Fractionation*—For preparation of digitonin-lysed cell fractions, cells were washed with PBS and suspended in PBS followed by lysis with 0.3 mg/ml digitonin for 3 min at 37 °C and centrifuged at 12,000 × *g* for 5 min at 4 °C. The pellet and supernatant fractions were used for immunoblot analysis with the pellet fraction including nuclei and heavy membranes and the supernatant fraction containing cytoplasm and light membranes.

For preparation of subcellular fractions, cells were washed with PBS and suspended in hypotonic solution (10 mM Hepes (pH 7.4), 10 mM $MgCl_2$, 42 mM KCl, 10 μM lactacystin) for 5 min on ice. Cells were lysed using a Dounce homogenizer and centrifuged at 600 × *g* for 10 min to collect crude nuclei that were further purified as described below. The supernatant was further centrifuged at 100,000 × *g* for 90 min. The pellet and supernatant were used as membrane and cytoplasmic fractions, respectively. The crude nuclear fraction was passed through a 27-gauge needle several times, extensively washed with hypotonic solution, and centrifuged through a 2 M sucrose cushion at 150,000 × *g* for 60 min. The pellet was used as a purified nuclear fraction. Nonidet P-40-treated nuclei were prepared by washing the purified nuclei with hypotonic solution containing 0.5% Nonidet P-40 to remove contaminating membranes.

*Antibodies*—Anti-active caspase-3 polyclonal (2622) and monoclonal (CS-1) antibodies, which recognize caspase-3-p12, were generated (see supplemental material). Anti-caspase-3 monoclonal antibody (C31720) was obtained from Transduction Laboratories; anti-caspase-3 polyclonal antibodies (sc-1224), anti-PKC δ polyclonal antibodies (sc-937), and anti-lamin B1 polyclonal antibodies (sc-6217) were from Santa Cruz Biotechnology; anti-active caspase-3 pAb (G7481) was from Promega; anti-green fluorescent protein (GFP) monoclonal antibody (8371) from Clontech; and anti-caspase-3 polyclonal antibodies (9662) was from Cell Signaling Technology.

*Fluorescence Microscopy*—For immunofluorescence analysis, cells were fixed with 3.7% formaldehyde in PBS for 10 min, washed with PBS twice, permeabilized in 0.5% Triton X-100 in PBS for 10 min, and washed with PBS twice. Cells were then incubated with primary antibodies in PBS containing 1% BSA overnight at 4 °C. After washing with PBS twice, cells were incubated with Texas red (TXRD)-, fluorescein isothiocyanate-, Alexa Fluor 488-, or Cy3-labeled secondary antibodies for 10 min at room temperature and washed with PBS twice. After staining nuclei with 10 μM Hoechst 33342 (Calbiochem), cells were examined under a fluorescence microscope (Leitz Laborlux) or a confocal laser scanning microscope (Carl Zeiss).

*Plasmid Constructions*—The wild type procaspase-3 cDNA fragment was cloned into the EcoRI site of pUC-CAGGS (17) to generate pCAG-casp3. To construct expression plasmids for caspase fused to the N terminus of GFP, PCR was carried out using caspase-3 and caspase-7 cDNAs as templates. The fragments encoding caspase-3 or caspase-7 were cloned into the EcoRI-BamHI site of pEGFP-N1 (Clontech) to generate pcasp3-Wt-GFP or pcasp7-Wt-GFP. To generate C163S, D175A, R64E, and R207E mutations, a PCR method employing mutagenic oligonucleotide primers was used. Caspase-3 cDNAs containing these mutations were cloned into the EcoRI-BamHI site of pEGFP-N1 to generate pcasp3-C163S-GFP, pcasp3-D175A-GFP, pcasp3-R64E-GFP, and pcasp3-R207E-GFP.

## RESULTS AND DISCUSSION

Although it has been widely accepted that procaspase-3 is cleaved to generate the active form in the cytoplasm, the enzymatic activity of capase-3-like proteases can be found in the nuclear fraction of apoptotic cells (18–20). It is, however, necessary to determine whether activated caspase-3 itself is present in the nuclei of apoptotic cells, as opposed to other caspases such as caspase-7 and -8 that can also cleave caspase-3 substrates (21, 22). The p17 subunit of active caspase-3 is detected not only in the cytoplasmic and mitochondrial fractions but also in the nuclear fraction of apoptotic cells (23). However, the localization of the p12 subunit of active caspase-3 remained to be determined, which is important, because caspase-3 enzymatic activity requires both p17 and p12 subunits. Therefore, we initially investigated the localization of the caspase-3-p12 subunit. HepG2 cells treated with or without an agonistic anti-Fas antibody were separated into pellet and supernatant fractions after lysis with digitonin, followed by immunoblotting (Fig. 1*A*). Although procaspase-3 was present in the supernatant fraction irrespective of induction of apoptosis, the caspase-3-p12 subunit was present in both the pellet fraction (including nuclei) and the supernatant fraction after induction of apoptosis. Subcellular fractionation was used to confirm the nuclear localization of active caspase-3 in apoptotic cells. Since active caspase-3 may be degraded by the ubiquitin-proteasome pathway (24–26), procaspase-3 was transiently overexpressed to elevate the expression levels of caspase-3, and the preparation of subcellular fractions was carried out in the presence of a proteasome inhibitor, lactacystin; PKC δ and lamin B1 were used as cytoplasmic and nuclear fraction markers, respectively. Normal non-transfected HepG2 cells (Fig. 1*B*, *left panel*) or transfected HepG2 cells treated with the anti-Fas antibody for 12 h (Fig. 1*B*, *right panel*) were fractionated into nuclear, membrane, and cytoplasmic fractions. Although the expression level of procaspase-3 in transfected cells was more than five times higher than in non-transfected cells, the cytoplasmic localization of procaspase-3 was unaffected by overexpression. Both caspase-3-p17 and caspase-3-p12 were detected not only in the cytoplasmic fraction but also in the nuclear fraction even after treatment with 0.5% Nonidet P-40 (Fig. 1*B*, *right panel*). These results strongly suggested that active caspase-3 was present in the nuclei of apoptotic cells.

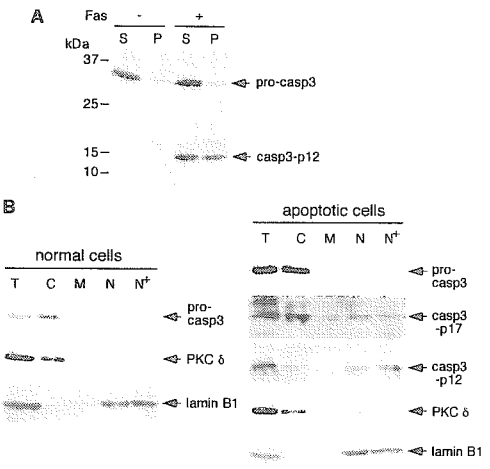


FIG. 1. **Nuclear localization of caspase-3-p17 and caspase-3-p12 subunits in apoptotic HepG2 cells.** *A*, detection of caspase-3-p12 subunit in HepG2 cells. HepG2 cells were treated with or without the anti-Fas antibody in the presence of actinomycin D for 12 h, and pellet (*P*) and supernatant (*S*) fractions were prepared after lysis with digitonin. Each fraction was subjected to SDS-PAGE and immunoblotted with anti-caspase-3 polyclonal antibodies (sc-1224 from Santa Cruz Biotechnology), which detect both procaspase-3 and caspase-3-p12. *B*, subcellular fractionation of normal (*left panel*) and apoptotic (*right panel*) HepG2 cells. Subcellular fractions from apoptotic HepG2 cells were prepared after transfection with pCAG-casp3 followed by incubation for 24 h and treatment with the anti-Fas antibody in the presence of actinomycin D for 12 h. Subcellular fractions, standardized to represent equal numbers of cells in each fraction, were subjected to SDS-PAGE and immunoblotted with anti-caspase-3 monoclonal antibody (C31720 from Transduction Laboratories), anti-caspase-3 antibody (9662 from Cell Signaling Technology), anti-caspase-3 polyclonal antibodies (sc-1224 from Santa Cruz Biotechnology), anti-PKC δ polyclonal antibodies, or anti-lamin B1 polyclonal antibodies. *T*, total cell lysate; *C*, cytoplasmic fraction; *M*, membrane fraction; *N*, purified nuclear fraction; $N^+$, purified nuclear fraction after treatment with 0.5% Nonidet P-40.

To directly assess the localization of active caspase-3, we prepared antibodies specific for active caspase-3-p12 subunit. Since procaspase-3 is processed at $Asp^{28}$ and $Asp^{175}$ sites to generate new N and C termini, we generated four affinity-purified polyclonal and three monoclonal antibodies that specifically recognize the newly exposed N-terminal region of caspase-3-p12 (see supplemental material). We also used the commercially available anti-active caspase-3 specific antibodies (G7481, Promega) that recognize the newly exposed C terminus of caspase-3-p17. Al-

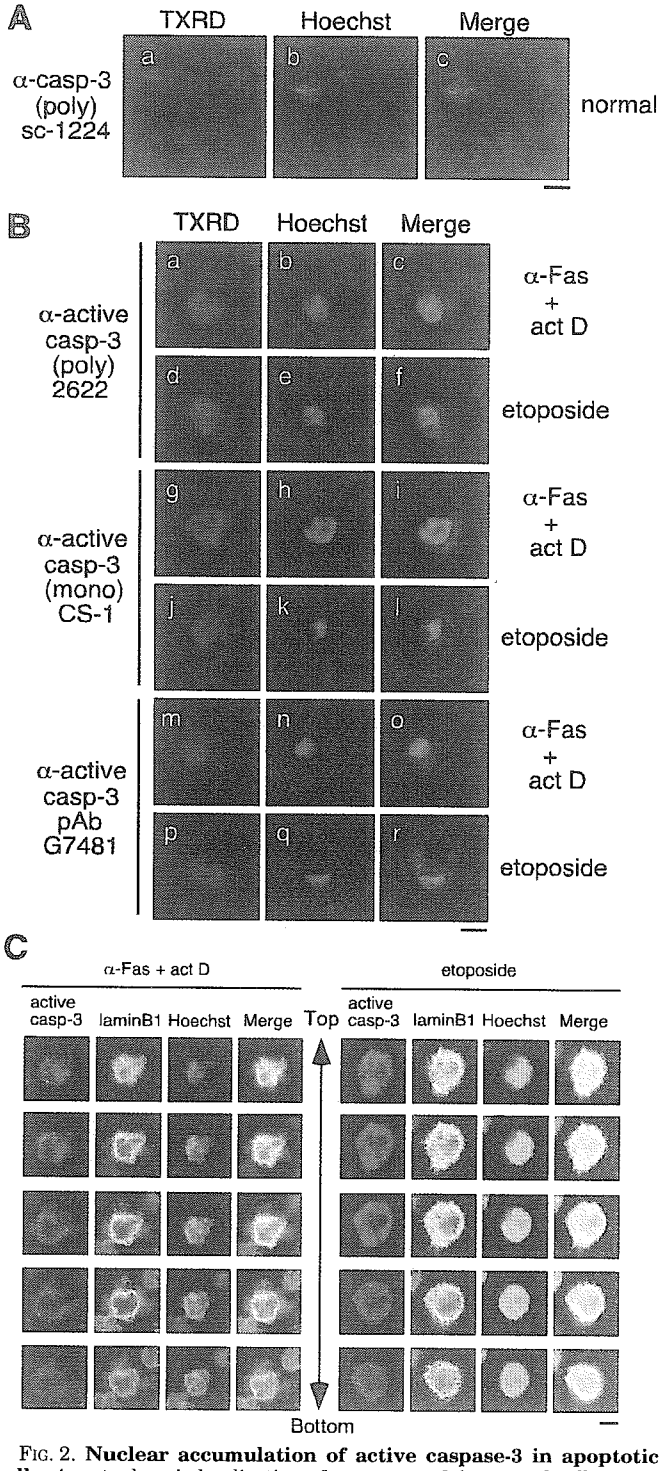


FIG. 2. **Nuclear accumulation of active caspase-3 in apoptotic cells.** *A*, cytoplasmic localization of procaspase-3 in normal cells. After fixation and permeabilization, HepG2 cells were incubated with anti-caspase-3 polyclonal antibodies (sc-1224 from Santa Cruz Biotechnology) and TXRD-labeled secondary antibodies (*panel a*), followed by staining the nuclei with Hoechst 33342 (*panel b*). Photographs were taken of the same fields in *panels a* and *b*, and merged images of TXRD and Hoechst staining are shown in *panel c*. *B*, accumulation of active caspase-3 around the apoptotic nuclei. HepG2 cells were treated with the anti-Fas antibody in the presence of actinomycin D (*act D*) for 12 h (*panels a–c, g–i,* and *m–o*) or with etoposide for 40 h (*panels d–f, j–l,* and *p–r*). After fixation and permeabilization, the cells were incubated with anti-active caspase-3 polyclonal antibodies (2622) (*panels a* and *d*), anti-active caspase-3 monoclonal antibody (CS-1) (*panels g* and *j*), anti-active caspase-3 pAb (G7481 from Promega) (*panels m* and *p*), and TXRD-labeled secondary antibodies (*panels a, d, g, j, m,* and *p*), followed by staining the nuclei with Hoechst 33342 (*panels b, e, h, k, n,* and *q*). Photographs were taken of the same fields in *panels a–c, d–f, g–i, j–l, m–o,* and *p–r*, and merged images of TXRD and Hoechst staining are shown in *panels c, f, i, l, o,* and *r*, respectively. *C*, detection of active caspase-3 in apoptotic nuclei. HepG2 cells were treated with the anti-Fas antibody in the presence of actinomycin D (*act D*) for 12 h or with etoposide for 40 h. After fixation and permeabilization, the cells were incubated with anti-active caspase-3 pAb (G7481 from Promega) and anti-lamin B1 polyclonal antibodies as a nuclear envelope marker, and Cy3- and Alexa Fluor 488-labeled secondary antibodies, followed by staining the nuclei with Hoechst 33342, and observed with confocal laser scanning microscope. The z-series of images from five sections are shown. *Bars*, 10 μm.

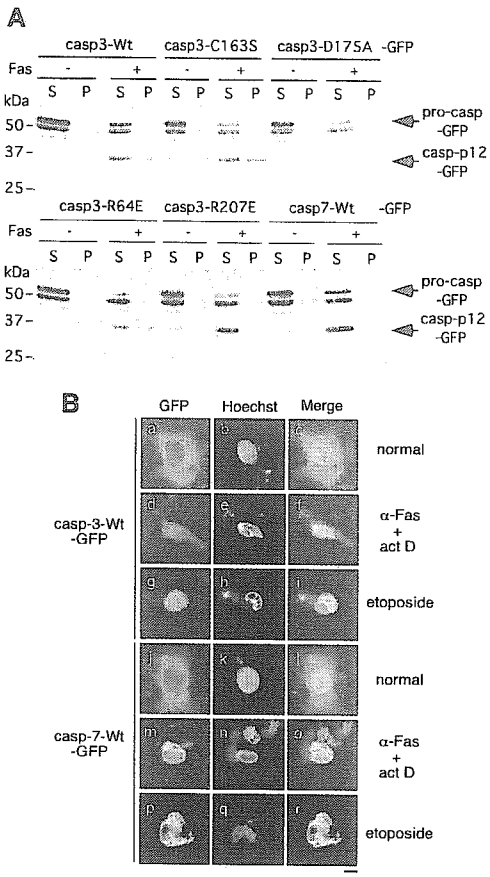


FIG. 3. **Nuclear translocation of active caspase-3 requires proteolytic activation and substrate recognition, but not catalytic activity.** *A*, localization of caspase-3- and caspase-7-GFP fusion proteins in HepG2 cells. One day before transfection, HepG2 cells were seeded at a density of $2 \times 10^5$ cells per well in 6-well dishes. In each well, 2 μg of plasmids expressing caspase-GFP fusion proteins were transfected and incubated for 24 h. After treatment with or without the anti-Fas antibody in the presence of actinomycin D (*act D*) for 12 h, cells were fractionated after lysis with digitonin and subjected to SDS-PAGE and immunoblotted with anti-GFP monoclonal antibody. *S*, supernatant fraction; *P*, pellet fraction. *B*, nuclear localization of caspase-3-, but not caspase-7-, GFP fusion protein in apoptotic cells with confocal laser scanning microscopy. One day before transfection, HepG2 cells were seeded at a density of $2 \times 10^5$ cells per 35-mm glass bottom dish. In each dish, 2 μg of pcasp3-Wt-GFP (*panels a–i*) or pcasp7-Wt-GFP (*panels j–r*) plasmids were transfected and incubated for 24 h. After treatment without (*panels a–c* and *j–l*) or with the anti-Fas antibody in the presence of actinomycin D (*act D*) for 12 h (*panels d–f* and *m–o*) or with etoposide for 40 h (*panels g–i* and *p–r*), GFP expression (*panels a, d, g, j, m,* and *p*) was observed with confocal laser scanning microscope after staining with Hoechst 33342 (*panels b, e, h, k, n,* and *q*). Photographs were taken of the same fields in *panels a–c, d–f, g–i, j–l, m–o,* and *p–r*, and merged images of GFP and Hoechst staining are shown in *panels c, f, i, l, o,* and *r*, respectively. *Bar*, 10 μm.

though procaspase-3 was detected in the cytoplasm of untreated normal cells (Fig. 2*A*), in most apoptotic cells stained with anti-active caspase-3 antibodies, which recognize the newly exposed N terminus of caspase-3-p12 (Fig. 2*B*, *panels a–l*) or the newly exposed C terminus of caspase-3-p17 (Fig. 2*B*, *panels m–r*), the signal was strongest around the condensed nucleus. To deter-

mine whether active caspase-3 is actually present in the nucleus, apoptotic cells were stained with the anti-active caspase-3 antibodies and antibodies against lamin B1, a nuclear envelope marker, and analyzed by confocal laser scanning microscopy (Fig. 2*C*). The signal for active caspase-3 was detected both in and around the condensed nuclei. Taken together, these results indicate that active caspase-3 is present not only in the cytoplasm but also in the nuclei of apoptotic cells.

To examine the molecular mechanisms governing translocation of caspase-3 from the cytoplasm into the nucleus, we constructed various procaspase-3 mutants fused with GFP. These constructs were transiently transfected into HepG2 cells. After treatment with or without the agonistic anti-Fas antibody to induce apoptosis, supernatant and pellet fractions were prepared after digitonin lysis and immunoblotted with the anti-GFP antibody (Fig. 3*A*). Although casp3-Wt-GFP was predominantly present in supernatant, like the unprocessed form before Fas treatment, proteolytically activated casp3-p12-GFP was recovered in both the supernatant and pellet fractions after Fas treatment (Fig. 3*A*). In contrast, caspase-7, another effector caspase, did not translocate to the nucleus, with both casp7-Wt-GFP and casp7-p12-GFP being detected only in the supernatant fraction irrespective of Fas treatment. Consistently, confocal laser scanning microscopy indicated that casp3-Wt-GFP was present in both cytoplasm and nuclei, whereas casp7-Wt-GFP was found only in the cytoplasm in apoptotic cells (Fig. 3*B*). These results suggested that the nuclear translocation of effector caspases is specific for caspase-3 and that the nuclear translocation of caspase-3 is an active process and not simply entail diffusion after disruption of the nuclear-cytoplasmic barrier.

To determine whether caspase-3 activation is needed for nuclear translocation, we constructed procaspase-3 mutants that cannot be activated, recognize substrates, or cleave substrates, respectively. Casp3-D175A-GFP, which is not activated due to mutation of the cleavage site between the p17 and p12 subunits, did not translocate after anti-Fas treatment, suggesting that the proteolytic activation of caspase-3 is necessary for its nuclear translocation (Fig. 3*A*). The three-dimensional structure of caspase-3 (27, 28) shows that $Arg^{64}$ and $Arg^{207}$ are essential for recognition of the P1 and P3 amino acids of the D*X*XD cleavage motif substrates, respectively. Cell fractionation analysis showed that casp3-R64E-GFP, but not casp3-R207E-GFP, translocated from cytoplasm to nuclei after Fas treatment, indicating that recognition of P3, but not P1, of a substrate(s) is necessary for nuclear translocation of active caspase-3 (Fig. 3*A*). Furthermore, casp3-C163S-GFP, in which the catalytic Cys is mutated, translocated from the cytoplasm into nuclei, indicating that substrate cleavage by caspase-3 is not essential for the translocation of active caspase-3. These results suggested that proteolytic activation and substrate recognition, but not substrate cleavage, are necessary for the nuclear translocation of active caspase-3.

Nuclear pore complexes (NPCs) mediate bidirectional transport between the cytoplasm and the nucleus (29). The NPC constitutes a passive diffusion channel, which allows the diffusion of ions, metabolites, and small proteins whose relative molecular mass is less than about 40 kDa. Proteins above the size limit can enter the nucleus by energy-dependent mechanisms. Caspase-3 lacks a typical consensus nuclear localization signal, and the active caspase-3 tetramer is too big to enter the nucleus passively. Recently, Faleiro and Lazebnik (16) reported that caspase-9 inactivates nuclear transport and increases the diffusion limit of the nuclear pore, leading to the entrance of caspase-3 into nuclei by diffusion. If caspase-3 enters the nucleus by simple diffusion, procaspase-3 as well as active caspase-3 and other caspases including caspase-7 would also be detected in the nuclear fraction of apoptotic cells. However, our data showed that neither procaspase-3 nor caspase-7 translocated into nuclei after apoptosis induction. Furthermore, active nuclear transport is required for the nuclear morphological changes induced by various apoptotic stimuli (30), and nuclear translocation of active caspase-3 required proteolytic activation and recognition of substrate-like protein(s). Therefore, we propose that the nuclear translocation of active caspase-3 is dependent on active nuclear transport. Identification of the substrate-like protein(s) which function as a carrier protein to transport active caspase-3 from the cytoplasm into nucleus in apoptotic cells is needed to clear the molecular mechanisms of nuclear translocation of active caspase-3.

*Acknowledgments*—We thank Drs. Yoshiteru Kobayashi and Shinji Tanahashi (Wako Pure Chemical Industries, Osaka, Japan) for cooperation in generating antibodies, Dr. Jeong-Hwa Lee for technical support in immunofluorescence analysis, Drs. Joel D. Leverson and Han-Kuei Huang for critical reading of the manuscript, Dr. Vishva M. Dixit for the pcDNA3/Yama plasmid, and Dr. Jun-ichi Miyazaki for the pUC-CAGGS plasmid.

REFERENCES

1. Alnemri, E. S., Livingston, D. J., Nicholson, D. W., Salvesen, G., Thornberry, N. A., Wong, W. W., and Yuan, J. (1996) *Cell* **87,** 171
2. Cryns, V., and Yuan, J. (1998) *Genes Dev.* **12,** 1551–1570
3. Thornberry, N. A., and Lazebnik, Y. (1998) *Science* **281,** 1312–1316
4. Earnshaw, W. C., Martins, L. M., and Kaufmann, S. H. (1999) *Annu. Rev. Biochem.* **68,** 383–424
5. Fernandes-Alnemri, T., Litwack, G., and Alnemri, E. S. (1994) *J. Biol. Chem.* **269,** 30761–30764
6. Tewari, M., Quan, L. T., O'Rourke, K., Desnoyers, S., Zeng, Z., Beidler, D. R., Poirier, G. G., Salvesen, G. S., and Dixit, V. M. (1995) *Cell* **81,** 801–809
7. Nicholson, D. W., Ali, A., Thornberry, N. A., Vaillancourt, J. P., Ding, C. K., Gallant, M., Gareau, Y., Griffin, P. R., Labelle, M., Lazebnik, Y. A., Mungay, N. A., Raju, S. M., Smulson, M. E., Yamin, T.-T., Yu, Y. L., and Miller, D. K. (1995) *Nature* **376,** 37–43
8. Kuida, K., Zheng, T. S., Na, S., Kuan, C., Yang, D., Karasuyama, H., Rakic, P., and Flavell, R. A. (1996) *Nature* **384,** 368–372
9. Woo, M., Hakem, R., Soengas, M. S., Duncan, G. S., Shahinian, A., Kagi, D., Hakem, A., McCurrach, M., Khoo, W., Kaufman, S. A., Senaldi, G., Howard, T., Lowe, S. W., and Mak, T. W. (1998) *Genes Dev.* **12,** 806–819
10. Zheng, T. S., Schlosser, S. F., Dao, T., Hingorani, R., Crispe, I. N., Boyer, J. L., and Flavell, R. A. (1998) *Proc. Natl. Acad. Sci. U. S. A.* **95,** 13618–13623
11. Enari, M., Sakahira, H., Yokoyama, H., Okawa, K., Iwamatsu, A., and Nagata, S. (1998) *Nature* **391,** 43–50
12. Liu, X., Li, P., Widlak, P., Zou, H., Luo, X., Garrard, W. T., and Wang, X. (1998) *Proc. Natl. Acad. Sci. U. S. A.* **95,** 8461–8466
13. Sahara, S., Aoto, M., Eguchi, Y., Imamoto, N., Yoneda, Y., and Tsujimoto, Y. (1999) *Nature* **401,** 168–173
14. Lechardeur, D., Drzymala, L., Sharma, M., Zylka, D., Kinach, R., Pacia, J., Hicks, C., Usmani, N., Rommens, J. M., and Lukacs, G. L. (2000) *J. Cell Biol.* **150,** 321–334
15. Fischer, U., Janicke, R. U., and Schulze-Osthoff, K. (2003) *Cell Death Differ.* **10,** 76–100
16. Faleiro, L., and Lazebnik, Y. (2000) *J. Cell Biol.* **151,** 951–959
17. Niwa, H., Yamamura, K., and Miyazaki, J. (1991) *Gene (Amst.)* **108,** 193–199
18. Martins, L. M., Mesner, P. W., Kottke, T. J., Basi, G. S., Sinha, S., Tung, J. S., Svingen, P. A., Madden, B. J., Takahashi, A., McCormick, D. J., Earnshaw, W. C., and Kaufmann, S. H. (1997) *Blood* **90,** 4283–4296
19. Mandal, M., Adam, L., and Kumar, R. (1999) *Biochem. Biophys. Res. Commun.* **260,** 775–780
20. Takemoto, K., Nagai, T., Miyawaki, A., and Miura, M. (2003) *J. Cell Biol.* **160,** 235–243
21. Thornberry, N. A., Rano, T. A., Peterson, E. P., Rasper, D. M., Timkey, T., Garcia-Calvo, M., Houtzager, V. M., Nordstrom, P. A., Roy, S., Vaillancourt, J. P., Chapman, K. T., and Nicholson, D. W. (1997) *J. Biol. Chem.* **272,** 17907–17911
22. Garcia-Calvo, M., Peterson, E. P., Leiting, B., Ruel, R., Nicholson, D. W., and Thornberry, N. A. (1998) *J. Biol. Chem.* **273,** 32608–32613
23. Zhivotovsky, B., Samali, A., Gahm, A., and Orrenius, S. (1999) *Cell Death Differ.* **6,** 644–651
24. Huang, H., Joazeiro, C. A., Bonfoco, E., Kamada, S., Leverson, J. D., and Hunter, T. (2000) *J. Biol. Chem.* **275,** 26661–26664
25. Suzuki, Y., Nakabayashi, Y., and Takahashi, R. (2001) *Proc. Natl. Acad. Sci. U. S. A.* **98,** 8662–8667
26. Chen, L., Smith, L., Wang, Z., and Smith, J. B. (2003) *Mol. Pharmacol.* **64,** 334–345
27. Rotonda, J., Nicholson, D. W., Fazil, K. M., Gallant, M., Gareau, Y., Labelle, M., Peterson, E. P., Rasper, D. M., Ruel, R., Vaillancourt, J. P., Thornberry, N. A., and Becker, J. W. (1996) *Nat. Struct. Biol.* **3,** 619–625
28. Wei, Y., Fox, T., Chambers, S. P., Sintchak, J., Coll, J. T., Golec, J. M. C., Swenson, L., Wilson, K. P., and Charifson, P. S. (2000) *Chem. Biol.* **7,** 423–432
29. Gorlich, D., and Mattaj, I. W. (1996) *Science* **271,** 1513–1518
30. Yasuhara, N., Eguchi, Y., Tachibana, T., Imamoto, N., Yoneda, Y., and Tsujimoto, Y. (1997) *Genes Cells* **2,** 55–64

ELSEVIER

European Journal of Cardio-thoracic Surgery 27 (2005) 117-121

EUROPEAN JOURNAL OF CARDIO-THORACIC SURGERY

www.elsevier.com/locate/ejcts

# BH4 peptide derivative from Bcl-xL attenuates ischemia/reperfusion injury thorough anti-apoptotic mechanism in rat hearts

Masamichi Ono[a], Yoshiki Sawa[a,*], Masahiro Ryugo[a], Alexei N. Alechine[a], Shigeomi Shimizu[b], Rie Sugioka[b], Yoshihide Tsujimoto[b], Hikaru Matsuda[a]

[a]Department of Surgery, Osaka University Graduate School of Medicine, 2-2 Yamadaoka, Suita, Osaka 565-0871, Japan
[b]Department of Post-Genomics and Diseases, Osaka University Graduate School of Medicine, 2-2 Yamadaoka, Suita, Osaka 565-0871, Japan

Received 18 May 2004; received in revised form 6 September 2004; accepted 9 September 2004

**Abstract**

**Objective**: To prevent apoptosis is thought to be promising for myocardial protection in cardiac surgery. Recently, we showed that BH4 domain of Bcl-xL is essential for the prevention of apoptosis, and that BH4 fused to HIV TAT protein (TAT-BH4) prevented apoptotic cell death. Then, we hypothesized TAT-BH4 may attenuate ischemia/reperfusion injury in rat hearts. **Methods**: The isolated rat hearts in the TAT-BH4 preconditioning group (BH4 group, $n=8$) or control group (C group, $n=8$) were subjected to warm ischemia (37 °C) for 30 min followed by 60 min of reperfusion using Langendorff perfusion system. **Results**: Left ventricular developed pressure and maximum $dP/dt$ after reperfusion were significantly improved in the BH4 group than those in the C group ($P<0.01$). Recovery of mitochondrial respiration was significantly better in the BH4 group ($P<0.05$). Moreover, expression of caspase-3 and TUNEL-positive myocardium were decreased in the BH4 group than those in the C group. **Conclusions**: These results demonstrated that TAT-BH4 attenuates myocardial ischemia/reperfusion injury through preventing myocardial apoptosis. Thus, TAT-BH4 may be a novel therapeutic agent for myocardial protection in cardiac surgery.


*Keywords:* Apoptosis; Cardiomyocytes; Ischemia/reperfusion injury; Heart surgery

## 1. Introduction

Recent advances in myocardial protection have improved the clinical results in open-heart surgery. However, severely critical cases associated with compromised heart, such as failing heart or post-ischemic conditions, still occur, and thus, further attempts to improve myocardial protection should be addressed.

Recently, a growing body of evidence have shown that apoptosis of myocardium is one of the major contributors to ischemic/reperfusion injury in experimental models [1-5] and even in humans after open-heart surgery [6,7]. Therefore, many attempts through molecular mechanism to attenuate apoptosis of myocardium in ischemia/reperfusion injury have been reported [8-15]. However, no pharmacological strategy has been reported to attenuate apoptosis in the heart. Moreover, strategy using gene transfection during ischemia has limitations because it takes few ours to express proteins after reperfusion, which is not suitable for clinical application of myocardial protection against acute ischemic reperfusion injury.

We recently demonstrated that the biochemical role of the conserved N-terminal homology domain (BH4) of Bcl-xL is essential for the prevention of apoptosis, with respect to the regulation of mitochondrial membrane permeability and found that BH4 was required for Bcl-xL to prevent cytochrome *c* release. Using a newly developed TAT protein transduction system, which is the protein transduction domain of human immunodeficiency virus type 1 Tat protein (HIV TAT protein), we also showed that the BH4 domain fused to TAT protein (TAT-BH4), effectively prevented apoptotic cell death in vitro [16], and showed feasibility of protein transduction into cells in vivo. Chen et al. demonstrated TAT-BH4 attenuated myocardial infarction in vivo [17]. Therefore, it is expected that preconditioning of TAT-BH4 may attenuate ischemia/reperfusion injury of the myocardium during open heart surgery.

In this study, we investigated whether the preconditioning of TAT-BH4 may attenuate ischemia/reperfusion injury in isolated rat heart model as a pre-clinical trial.

* Corresponding author. Tel.: +81 6 6879 3151; fax: +81 6 6879 3163.
*E-mail address:* sawa@surg1.med.osaka-u.ac.jp (Y. Sawa).

1010-7940/$ - see front matter © 2004 Elsevier B.V. All rights reserved.
doi:10.1016/j.ejcts.2004.09.025

## 2. Method

### 2.1. Test compounds

TAT-BH-4 protein and TAT mutant protein were provided by Shionogi Pharmacy Co., Ltd, Osaka, Japan. The proteins were dissolved in DMSO to the concentration of 5 μg/μl before use.

### 2.2. Pharmacological preconditioning and rat ischemia model

Sixteen Sprague-Dawley rats (300 g, male) were used for this study. Humane animal care complied with the 'Principle of Laboratory Animal Care' formulated by the National Society for Medical Research and the 'Guide for the Care and Use of Laboratory Animals' prepared by the Institute of Laboratory Animal Resource and published by the Institutes of Health (NIH Publication No. 86-23, revised 1985). The rats were divided into the control group (C group, $n=8$), and the TAT-BH-4 group (BH4 group, $n=8$). All rats were anesthetized by intra-peritoneal injection of sodium pentobarbital (50 mg/kg). Following 10 min of the injection and anticoagulation with heparin (200 USP units, intra-peritoneally), the hearts were quickly excised and perfused with modified Krebs-Henseleit buffer (120.0 mM NaCl, 4.5 mM KCl, 20.0 mM $NaHCO_3$, 1.2 mM $KH_2PO_4$, 1.2 mM $MgCl_2$, 2.5 mM $CaCl_2$, and 10.0 mM glucose: gassed with 95% $O_2$+5% $CO_2$ to obtain pH 7.4 at 37 °C) at the pressure equal to 1 m $H_2O$ by means of a Langendorff apparatus. A thin-wall latex balloon was inserted into the left ventricle through the left atrium to monitor left ventricular pressure and to control left ventricular volume. After stabilization, heart rate (HR), left ventricular developed pressure (LVDP), maximum $dP/dt$ (max $dP/dt$), and coronary flow (CF) were measured with LV diastolic pressure stabilized at 10 mmHg. Then, 100 μg (20 μl) of TAT-BH4 protein (BH4 group) or TAT mutant protein (C group), diluted by 5 ml of modified Krebs-Henseleit buffer, were administered through side port of apparatus at the speed of 1 ml/min. The hearts were then subjected to global ischemia at 37 °C for 30 min, followed by 60 min of reperfusion. The balloon was deflated during ischemia. The indices of cardiac function were continuously measured after reperfusion and analyzed using Polygraph System (Nihon Kouden, Japan). After 60 min of reperfusion, frozen sections of the hearts were made and stored at −80 °C for further assessment.

### 2.3. The recovery of mitochondrial respiration

Mitochondria were isolated from the hearts after reperfusion in 0.3 M mannitol/10 mM potassium Hepes, pH 7.4/0.2 mM EGTA, pH 7.4/0.1% fatty acid-free BSA by centrifugation at 2500×$g$ for 10 min. The mitochondria were washed twice with this medium without EGTA to which 5 mM potassium phosphate was added and then suspended in it. Mitochondrial respiration was measured with an $O_2$ electrode, and the recovery of respiration was defined as the ratio of mitochondrial respiration in the hearts after reperfusion to the hearts before ischemia.

### 2.4. Western blotting analysis of active caspase-3

To evaluate the activation of apoptotic cascade after reperfusion, western blot analysis for detection of active caspase-3 was performed using the frozen section samples after 60 min of reperfusion. We used active caspase-3 rabbit polyclonal IgG antibody, and anti-rabbit secondary antibody conjugated to horseradish peroxidase and Phototope-HRP Western detection kit. The degree of the protein expression was semi-quantitatively evaluated with computed densitometry (Scion Image: Windows; Microsoft Corporation).

### 2.5. Histological analysis of apoptosis

The frozen section samples after 60 min of reperfusion were prepared for histological analysis. TUNEL staining was performed using Terminal Deoxynucleotidyle Transferase Mediated UTP-Biotin In Situ Nick-End Labeling (Tunnel Intergen Kit) according to the manufacturer's instruction. Quantitative assessment was calculated as a percentage of TUNEL-positive nuclei.

### 2.6. Statistical analysis

All data are expressed as mean±standard error of the means (SEM). Scores were compared using an unpaired Student's $t$ test. A $P$ value of less than 0.05 was considered statistically significant.

## 3. Results

### 3.1. Recovery of cardiac function after global ischemia

To evaluate the efficacy of TAT-BH4 protein, we firstly analyzed cardiac function after global warm ischemia and reperfusion. The time course of percent recovery of LVDP after global ischemia (37 °C, 30 min) was shown in Fig. 1A. In comparison with the C group, a significant improvement of the percent recovery of LVDP was observed in the BH4 group at 10, 20, 30, 40, 50, and 60 min after reperfusion. The value after 60 min of reperfusion in the C group was 47±4%, and was significantly improved to 72±4% in the BH4 group ($P<0.01$).

The time course of percent recovery of max $dP/dt$ after global ischemia was shown in Fig. 1B. In comparison with the C group, a significant improvement of the index was observed in the BH4 group at 20, 30, 40, 50, and 60 min after reperfusion. The value after 60 min of reperfusion in the C group was 36±9%, and was significantly improved to 71±3% in the BH4 group ($P<0.01$). CF after 60 min reperfusion was also significantly higher in the BH4 group compared with the C group (13.8±0.9 vs. 8.9±1.2 ml/min; $P<0.01$) (Fig. 1C).

### 3.2. Mitochondrial function by the recovery of respiration

Consistently, mitochondrial function assessed by the recovery of respiration markedly increased (C; 30±5, B; 77±10%, $P<0.05$) (Fig. 2).

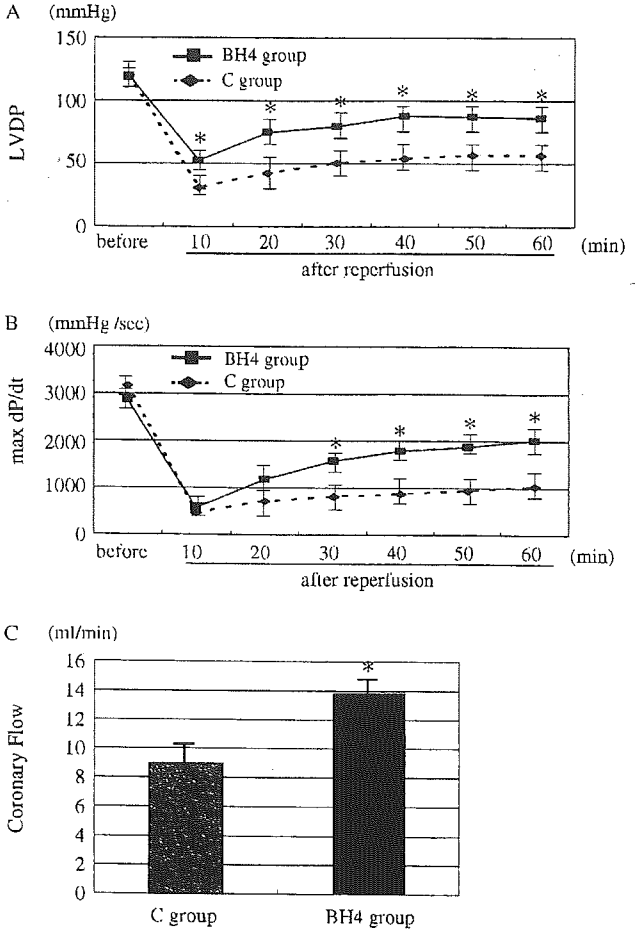


Fig. 1. Cardiac function after reperfusion. The isolated hearts from the two groups were subjected to 30 min of normothermic global ikschemia followed by 60 min of reperfusion. Better recovery of LVDP (A) and maximum $dP/dt$ (B) after ischemia was shown in the BH4 group than in the C group. Data are expressed as percentage of basal value before ischemia. $^{**}P<0.01$, $^{*}P<0.05$. The coronary flow after reperfusion (C): the coronary flow 60 min after reperfusion was measured. $^{*}P<0.05$. $n=8$ in each group. All values are expressed as mean ± SEM.

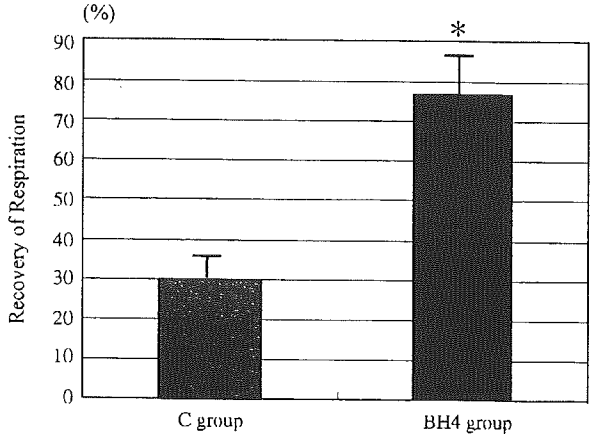


Fig. 2. The recovery of respiration: the recovery of mitochondrial respiration 60 min after reperfusion was measured. $^{*}P<0.05$. $n=8$. All values are expressed as mean ± SEM.

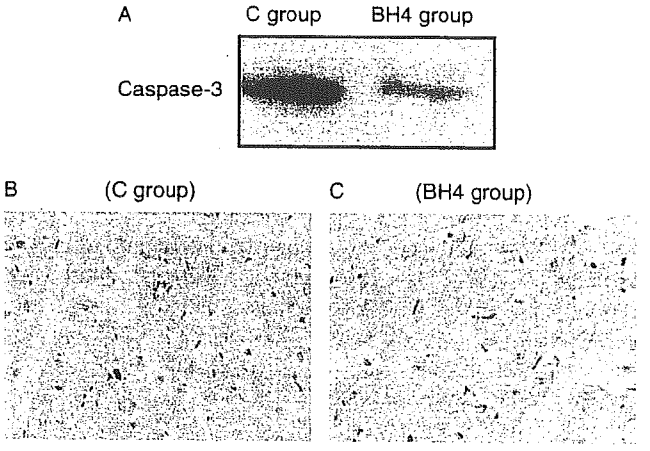


Fig. 3. Apoptosis of the myocardium after reperfusion. The myocardial expression of caspase-3 was significantly lower in the BH4 group than in the C group (A). The TUNEL-positive cardiomyocytes has detected in the control (B), but not in the BH4 group (C).

### 3.3. Evaluation of apoptosis by active caspase-3 expression and TUNEL staining

Then, we evaluated the apoptosis of the myocardium by Western blotting of active caspase-3 and TUNEL staining of the myocardium 60 min after reperfusion. The western blotting analysis for caspase-3 showed lower expression of active caspase-3 in the BH4 group compared with the C group (Fig. 3A). According to semi-quantitative analysis with computed densitometry, the BH4 group showed 1/3-1/4 less caspase-3 expression than the C group. The TUNEL staining of the heart section showed none of TUNEL-positive cells in the BH4 group (Fig. 3C), but significantly positive in the C group (Fig. 3B). The percent TUNEL-positive cells in the C group was 2.2 ± 0.3% of all cardiomyocytes, whereas TUNEL-positive cells could not be seen in BH4 group ($P<0.01$).

## 4. Discussion

In the present report, we showed cardioprotective effect of TAT-BH4; a novel linkage of the protein transduction domain of HIV TAT to the functional domain of Bcl-xL. The recovery of cardiac function, mitochondrial respiration of the myocardium after ischemia/reperfusion was significantly better by TAT-BH4 administration. Moreover, TAT-BH4 attenuated caspase-3 expression and reduced apoptosis of cardiomyocytes.

Apoptosis is an actively regulated process of cellular self-destruction, thereby distinct from necrosis. It encloses mitochondrial changes with characteristic release of substances promoting apoptosis like cytochrome *c*. Downstream in the apoptotic program the caspase cascade such as caspase-3 is activated, followed by cytoskeletal alterations, chromatin condensation, and DNA fragmentation, culminating in cell death. Previous experimental studies have well shown that apoptosis of cardiomyocytes is induced from early stage of ischemia/reperfusion, playing an important role for the cardiac dysfunction [1-5]. Using isolated rat

heart model, Scarabelli et al. [4] demonstrated that apoptosis (caspase-3 and TUNEL-positive nuclei) is seen in the very early stages (5 min of reperfusion) of ischemia/reperfusion in both endothelial cells and cardiomyocytes. Previous clinical studies also demonstrated apoptosis is evident early after ischemia/reperfusion during open-heart surgery. Schmitt et al. [6] showed that cytochrome c release and TUNEL-positive myocytes were increased even at the time of weaning from extracorporeal circulation (40 min of reperfusion), and apoptotic index showed a negative correlation with left ventricular function during surgery. Wu et al. [7] demonstrated percent TUNEL-positive myocytes was significantly increased even just after cross-claming release (10 min of reperfusion). These findings are consistent with our result of increased caspase-3 activities and TUNEL-positive myocytes 60 min after reperfusion.

There are many reports to attenuate ischemia/reperfusion injury through inhibiting apoptosis [8-15]. Several reports demonstrated the effects of gene transfer of anti-apoptotic gene [8-12]. Huang et al. [11] showed the effects of Bcl-xL gene transfer in rat model, but gene transfection needs a couple of days to gene expression, so this method is not suitable clinically for cardio-protection during open heart surgery. Other reports [13-15] showed the effects of anti-apoptotic protein administration such as caspase inhibitor [13], but this method needs frequent or continuous administration of relatively high dose of drugs during ischemia and reperfusion, which might induce deleterious side effects in other organs. Compared with the previous methods, TAT-BH4 administration before ischemia has some advantages over previous approach, because administration of essential domain for Bcl-xL by TAT system enables effective protein transduction into the target cells and potentiate immediately after reperfusion.

Our results showed that BH4 administration suppressed apoptotic cascade, resulting in improvement of cardiac function from early stage of reperfusion. Caspase-3 expression, an important molecule in the cellular suicide cascade, was minimal and no TUNEL-positive cells were seen in the BH4 group. The mechanism that BH4 inhibits apoptosis has already been demonstrated in our previous report [16]. BH4 of Bcl-xL is essential for inhibition of apoptosis with respect to the regulation of mitochondrial membrane permeability and is able to inhibit both voltage-dependent anion channel activity even in the presence of Bax and apoptotic mitochondrial membrane permeability loss. The mechanisms of this rapid effect for cardiac function by inhibiting apoptosis is remain to be addressed. Cheng et al. [18] reported that even such a small number of cells affected by apoptosis may have a significant impact on cardiac contractility, because single-cell death impinges upon the force-generating ability of neighboring cells that are still viable but stunned. Relatively few apoptotic cells may substantially impair side-to-side slippage of myocytes, resulting in a disproportionate and much more severe cardiac dysfunction. As a result, TAT-BH4 administration before ischemia inhibited almost completely apoptotic cascade during ischemia/reperfusion, contributing improvement of cardiac function from the early stage of reperfusion.

The HIV TAT protein: the amino-acid transduction domain of TAT contains a domain that facilitates protein transduction across cellular membranes. Although the exact mechanism of protein transduction across cellular membranes remains unknown, TAT-mediated protein transduction has been shown to occur even at 4 °C and is receptor independent [19]. These characteristics of TAT protein are also thought to be promising for protein transduction during open heart surgery.

These well known mechanisms of TAT-BH4 preventing mitochondrial function and apoptosis characterizes the promising possibility for clinical appreciation of this agent in cardiac surgery. Our data have strongly supported the importance of further investigation for clinical appreciation of this agent in future.

In conclusion, we obtained evidence that TAT-BH4 attenuates myocardial ischemia/reperfusion injury via inhibition of apoptosis of the myocardium. Thus, TAT-BH4 may be a novel therapeutic strategy for the protection of post-operative cardiac dysfunction in cardiovascular surgery.

## References

[1] Gill C, Mestril R, Samali A. Losing heart: the role of apoptosis in heart disease—a novel therapeutic target? Fed Am Soc Exp Biol J 2002;16:135-46.

[2] Freude B, Masters TN, Robicsek F, Fokin A, Kostin S, Zimmermann R, Ullmann C, Lorenz-Meyer S, Schaper J. Apoptosis is initiated by myocardial ischemia and executed during reperfusion. J Mol Cell Cardiol 2002;32:197-208.

[3] Vazquez-Jimenez JF, Qing M, Hermanns B, Klosterhalfen B, Woltje M, Chakupurakal R, Schumacher K, Messmer BJ, von Bernuth G, Seghaye MC. Moderate hypothermia during cardiopulmonary bypass reduces myocardial cell damage and myocardial cell death related to cardiac surgery. J Am Coll Cardiol 2001;38:1216-23.

[4] Scarabelli T, Stephanou A, Rayment N, Pasini E, Comini L, Curello S, Ferrari R, Knight R, Latchman D. Apoptosis of endothelial cells precedes myocyte cell apoptosis in ischemia/reperfusion injury. Circulation 2001;104:253-6.

[5] Gottlieb RA, Burleson KO, Kloner RA, Babior BM, Engler RL. Reperfusion injury induces apoptosis in rabbit cardiomyocytes. J Clin Invest 1994;94:1621-8.

[6] Schmitt JP, Schroder J, Schunkert H, Birnbaum DE, Aebert H. Role of apoptosis in myocardial stunning after open heart surgery. Ann Thrac Surg 2002;73:1229-35.

[7] Wu ZK, Laurikka J, Saraste A, Kyto V, Pehkonen EJ, Savunen T, Tarkka MR. Cardiomyocyte apoptosis and ischemic preconditioning in open heart operations. Ann Thrac Surg 2003;76:528-34.

[8] Sawa Y, Morishita R, Suzuki K, Kagisaki K, Kaneda Y, Maeda K, Kadoba K, Matsuda H. A novel strategy for myocardial protection using in vivo transfection of cis element 'decoy' against NFκB binding site: evidence for a role of NFκB in ischemia/reperfusion injury. Circulation 1997;96(suppl):II-280-II-285.

[9] Suzuki K, Murtuza B, Smolenski RT, Sammut IA, Suzuki N, Kaneda Y, Yacoub MH. Overexoression of interleukin-1 receptor antagonist provides cardioprotection against ischemia-reperfusion injury associated with reduction in apoptosis. Circulation 2001;104(suppl I):I-308-I-313.

[10] Suzuki K, Murtuza B, Sammut IA, Latif N, Jayakumar J, Smolenski RT, Kaneda Y, Sawa Y, Matsuda H, Yacoub MH. Heat shock protein 72 enhances manganese superoxide dismutase activity during myocardial ischemia-reperfusion injury, associated with mitochondrial protection and apoptosis reduction. Circulation 2002;106(suppl):I-270-I-276.

[11] Huang J, Ito Y, Morikawa M, Uchida H, Kobune M, Sasaki K, Abe T, Hamada H. Bcl-xL gene transfer protects the heart against ischemia/reperfusion injury. Ann Thrac Surg 2002;73:1229-35.

[12] Kato K, Yin H, Agata J, Yoshida H, Chao L, Chao J. Adrenomedullin gene delivery aattenuates myocardial infarction and apoptosis after ischemia and reperfusion. Ann J Physiol Heart Circ Physiol 2003;285:H1506-H14.
[13] Yaoita H, Ogawa K, Maehara K, Maruyama Y. Attenuation of ischemia/reperfusion injury in rats by a caspase inhibitor. Circulation 1998;97: 276-81.
[14] Grunenfelder J, Miniati DN, Murata S, Falk V, Hoyt EG, Robbins RC. Upregulation of Bcl-2 through caspase-3 inhibition ameriolates ischemia/reperfusion injury in rat cardiac allografts. Circulation 2001; 104(suppl):I-202-I-206.
[15] Maejima Y, Adachi S, Ito H, Nobori K, Tamamori-Adachi M, Isobe M. Nitric Oxide inhibits ischemia/reperfusion-induced myocardial apoptosis by modulation cyclin A-associated kinase activity. Cardiovasc Res 2003;59: 308-20.
[16] Shimizu S, Konishi A, Kodama T, Tsujimoto Y. BH4 domain of antiapoptotic Bcl-2 family members closes voltage-dependent anion channel and inhibits apoptotic mitochondrial changes and cell death. Proc Natl Acad Sci USA 2000;97:3100-5.
[17] Chen M, Won DJ, Krajewski S, Gottlieb RA. Calpain and mitochondria in ischemia/reperfusion injury. J Biol Chem 2002; 277:29181-6.
[18] Cheng W, Li B, Kajstura J, Wolin MS, Sonnenblick EH, Hintze TH, Olivetti G, Anversa P. Stretch-induced programmed myocytes cell death. J Clin Invest 1995;96:2247-59.
[19] Gustafsson AB, Sayen MR, Williams SD, Crow MT, Gottlieb RA. TAT protein transduction into isolated perfused hearts: TAT-apoptosis repressor with caspase recruitment domain is cardioprotective. Circulation 2002;106:735-9.

# Cyclophilin D-dependent mitochondrial permeability transition regulates some necrotic but not apoptotic cell death

Takashi Nakagawa[1,2,4], Shigeomi Shimizu[1,4], Tetsuya Watanabe[3], Osamu Yamaguchi[3], Kinya Otsu[3], Hirotaka Yamagata[1], Hidenori Inohara[2], Takeshi Kubo[2] & Yoshihide Tsujimoto[1,4]

[1]*Laboratory of Molecular Genetics, Department of Post-Genomics and Diseases,* [2]*Department of Otolaryngology and Sensory Organ Surgery and* [3]*Department of Internal Medicine and Therapeutics, Osaka University Medical school, 2-2 Yamadaoka, Suita, Osaka 565-0871, Japan*

[4]*Solution-Oriented Research for Science and Technology (SORST), Japan Science and Technology Corporation, 2-2 Yamadaoka, Suita, Osaka 565-0871, Japan*

**Mitochondria play an important role in energy production, $Ca^{2+}$ homeostasis and cell death. In recent years, the role of the mitochondria in apoptotic and necrotic cell death has attracted much attention[1,2]. In apoptosis and necrosis, the mitochondrial permeability transition (mPT), which leads to disruption of the outer mitochondrial membrane and mitochondrial dysfunction, is considered to be one of the key events, although its exact role in cell death remains elusive. We therefore created mice lacking cyclophilin D (CypD), a protein considered to be involved in the mPT, to analyse its role in cell death. CypD-deficient mice were developmentally normal and showed no apparent anomalies, but CypD-deficient mitochondria did not undergo the cyclosporin A-sensitive mPT. CypD-deficient cells died normally in response to various apoptotic stimuli, but showed resistance to necrotic cell death induced by reactive oxygen species and $Ca^{2+}$ overload. In addition, CypD-deficient mice showed a high level of resistance to ischaemia/reperfusion-induced cardiac injury. Our results indicate that the CypD-dependent mPT regulates some forms of necrotic death, but not apoptotic death.**

The mitochondrial permeability transition (mPT) is a regulated $Ca^{2+}$-dependent increase in the permeability of the mitochondrial membrane, which results in a loss in mitochondrial membrane potential ($\Delta\Psi$) mitochondrial swelling and rupture of the outer membrane[3]. The mPT is thought to occur after the opening of a channel, termed the permeability transition pore, which putatively consists of a voltage-dependent anion channel, an adenine nucleotide translocator, CypD, and some other molecule(s)[4]; however, an essential role for the adenine nucleotide translocator in the mPT is a matter of recent controversy[5,6].

CypD is a mitochondrial member of the cyclophilin family of peptidyl prolyl-*cis*, *trans*-isomerases (PPIases) and has a crucial role in protein folding[7]. It has been suggested that CypD is involved in regulating the mPT, on the basis of the observation that cyclosporin A (CsA), a specific inhibitor of cyclophilin family activity, blocks the mPT[8]. A CsA-insensitive mPT has also been suggested, although the molecular mechanism is completely unknown[9]. It has been shown that some forms of apoptosis are significantly inhibited by CsA, suggesting a role for CsA-sensitive mPT in apoptosis[2,4]. The mPT is also implicated in the remodelling of mitochondrial structure with mobilization of cytochrome *c* stores in cristae during apoptosis[10]. To determine whether CypD has a crucial role in the CsA-sensitive mPT, and to investigate whether the mPT is a key regulator of cell death, we created CypD-deficient mice by gene targeting (see Supplementary Fig. 1a–c). The absence of cyclophilin D protein in CypD-deficient mice was verified by western blotting (see Fig. 1a and Supplementary Fig. 1d). CypD-deficient mice were born at the expected mendelian frequency, developed normally, and did not have any detectable phenotypic anomalies.

To examine the role of CypD in the mPT, mitochondria were isolated from the livers of CypD-deficient mice and control littermates. The mitochondria showed no significant change in respiration rate in the absence of CypD (see Supplementary Fig. 2). As shown in Fig. 1a, PPIase activity was absent in CypD-deficient mitochondria, but not in control mitochondria, indicating that CypD is the major PPIase in the mitochondria. When control mitochondria were treated with 50 $\mu$M $Ca^{2+}$, the mPT occurred, as shown by mitochondrial swelling (Fig. 1b) and loss of $\Delta\Psi$ (Fig. 1c). These phenomena were not observed in CypD-deficient mitochondria (Fig. 1b, c). To examine the extent of mPT inhibition as a consequence of CypD-deficiency, successive doses of $Ca^{2+}$ were added to the mitochondria. $\Delta\Psi$ was lost after two additions of 50 $\mu$M $Ca^{2+}$ to control mitochondria, but it was still maintained after seven additions of $Ca^{2+}$ to CypD-deficient mitochondria (Fig. 1d). We investigated whether the absence of $Ca^{2+}$-induced mPT in CypD-deficient mitochondria was due to disturbance of $Ca^{2+}$ uptake. As shown in Fig. 1e, the extra-mitochondrial $Ca^{2+}$ concentration increased transiently, and rapidly returned to basal levels after each successive addition of $Ca^{2+}$ to CypD-deficient mitochondria, indicating normal $Ca^{2+}$ uptake by the mitochondria. Up to concentrations of 500 $\mu$M $Ca^{2+}$, most of the $Ca^{2+}$ was taken up by CypD-deficient mitochondria (Fig. 1e, f). Next, we analysed CypD-deficient mitochondria in the presence of much higher concentrations of $Ca^{2+}$, which can induce CsA-insensitive mPT[9]. Addition of more than 1 mM $Ca^{2+}$ induced swelling, collapse of $\Delta\Psi$, and impaired $Ca^{2+}$ uptake even in CypD-deficient mitochondria (Fig. 1f and Supplementary Fig. 3), and all of these events were insensitive to CsA, even when it was added to CypD-deficient mitochondria (see Supplementary Fig. 3). Taken together, these results suggest that the mPT induced by low doses of $Ca^{2+}$ is completely inhibited in CypD-deficient mitochondria, and that CypD is not involved in the CsA-insensitive increase in membrane permeability induced by high doses of $Ca^{2+}$. Furthermore, the addition of other mPT inducers, such as $H_2O_2$ and atractyloside, did not trigger the mPT in CypD-deficient mitochondria (see Supplementary Fig. 4).

In many forms of apoptosis, BH3-domain-containing proteins of the Bcl-2 family ('BH3-only' proteins) transduce apoptotic signals to the mitochondria, and induce cytochrome *c* release in a Bax/Bak-dependent manner[11]. Whether the CsA-sensitive mPT is involved in apoptotic cytochrome *c* release is controversial[12–15]. To address this question, we added recombinant Bid (rBid), one of the BH3-only proteins, to CypD-deficient and control mitochondria. As shown in Fig. 1g (top panel), CypD deficiency had no effect on rBid-induced cytochrome *c* release, which was different from the result in Bak-deficient mitochondria (Fig. 1g, bottom panel). Bad (another BH3-only protein, data not shown) and rBax (Fig. 1g; second panel), were also found to induce cytochrome *c* release equally in both CypD-deficient and control mitochondria. In contrast, $Ca^{2+}$-induced cytochrome *c* release was markedly reduced in CypD-deficient mitochondria (Fig. 1g; third panel). Interestingly, Bak deficiency did not have any effect on $Ca^{2+}$-induced cytochrome *c* release (Fig. 1g, bottom panel). Together, these data indicate that the mPT is involved in cytochrome *c* release induced by $Ca^{2+}$, but not by pro-apoptotic BH3-only proteins or Bax.

The results described above raise the possibility that the mPT might be involved in cell death due to mPT inducers (including $Ca^{2+}$ overload and reactive oxygen species), but is not involved in the common apoptotic pathway to which BH3-only proteins and Bax/Bak are committed. We first examined the responses of CypD-deficient cells to these death stimuli. As shown in Fig. 2a, control and CypD-deficient thymocytes underwent comparable levels of apoptosis when exposed to various apoptotic stimuli. Similar findings were also obtained when murine embryonic fibroblast cells (MEFs) and hepatocytes from CypD-deficient mice

were treated with various apoptotic reagents (Fig. 2b, c), and when these cells were transfected with DNA encoding Bax or a truncated form of Bid (tBid; Fig. 2d, e). Moreover, apoptotic death of intestinal epithelial cells also occurred equally in control and CypD-deficient mice subjected to X-ray irradiation (Fig. 2f). These results indicate that CypD-dependent (CsA-sensitive) mPT is not involved in the common apoptotic pathway.

Next, we tested control and CypD-deficient MEFs for cell death after exposure to $H_2O_2$. CypD-deficient MEFs were more resistant to $H_2O_2$-induced cell death than control cells as assessed by a CTB (cell titre blue) assay, which measures the metabolic activity of viable cells (Fig. 3a), and by Annexin-V staining (data not shown). $H_2O_2$-induced cell death is predominantly due to necrosis, based on the following observations: a lack of caspase activation (Fig. 3b), no effect of a caspase inhibitor (Fig. 3a), early disruption of the plasma membrane (Fig. 3c), and finally, no nuclear or oligonucleosomal DNA fragmentation (Fig. 3c and data not shown). Similar results for $H_2O_2$-induced cell death were also obtained using CypD-deficient hepatocytes (Fig. 3d and data not shown).

We also examined the effect of CypD on cell death induced by A23187, a $Ca^{2+}$ ionophore. CypD-deficient hepatocytes showed significant resistance to A23187-induced cell death (Fig. 3e). Like $H_2O_2$-induced cell death, A23187-induced cell death was not accompanied by caspase activation (Fig. 3f), so this type of

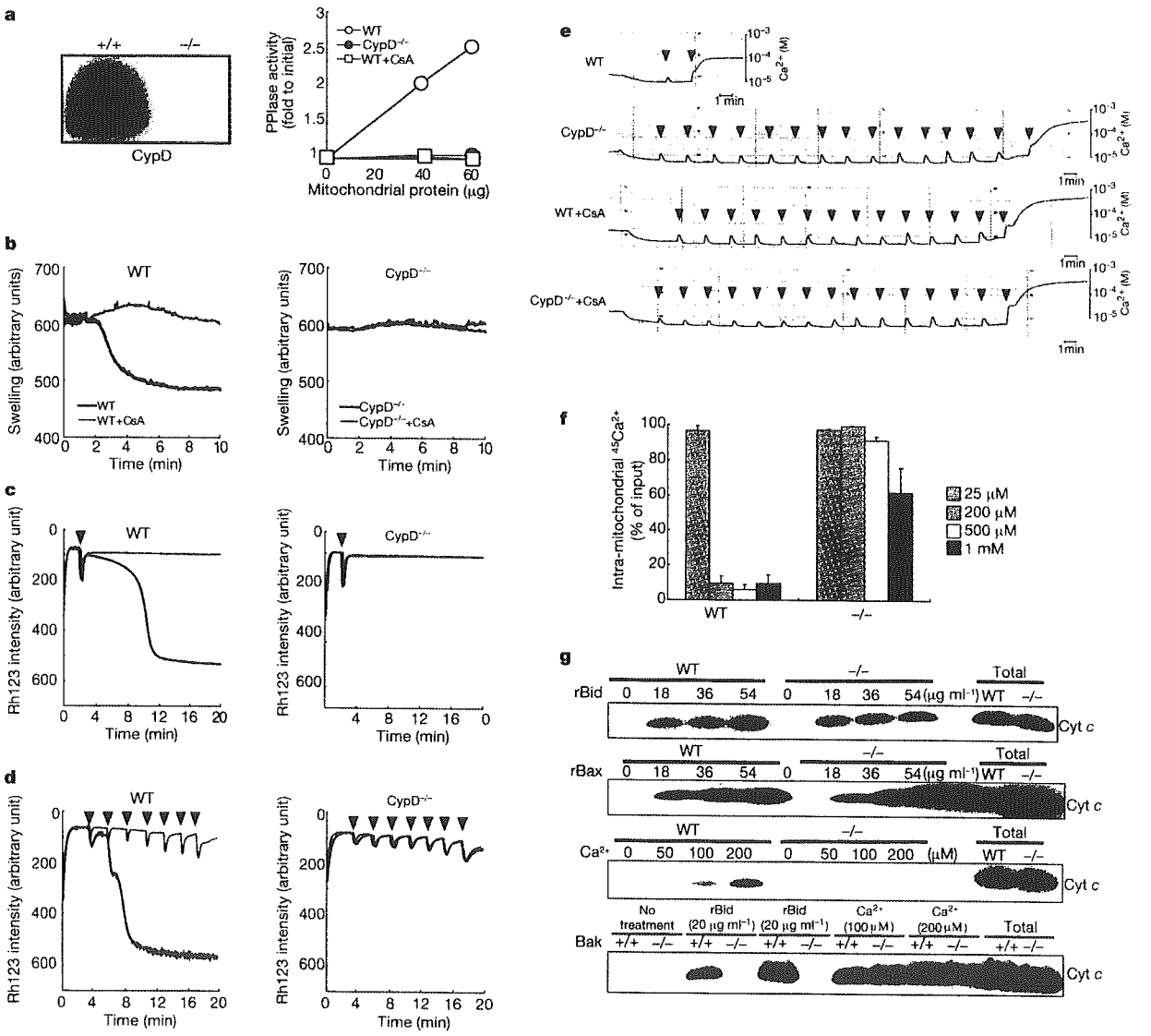


**Figure 1** Absence of mPT in CypD-deficient ($CypD^{-/-}$) mitochondria. **a**, Absence of CypD protein and PPIase activity in Cyp $D^{-/-}$ mitochondria. WT, wild type. **b**, **c**, Absence of mPT in $CypD^{-/-}$ mitochondria. Isolated wild-type (WT, left column) or $CypD^{-/-}$ (right column) mitochondria were incubated with 50 μM $Ca^{2+}$ in the presence (pink) or absence (blue) of 1 μM CsA, and monitored for (**b**) swelling (by light scatter) or (**c**) $\Delta\Psi$ (by Rh123 intensity), see Methods. Loss of $\Delta\Psi$ causes release of Rh123 from the mitochondria, resulting in increased Rh123 intensity. **d**, **e**, CypD deficiency prevents $Ca^{2+}$-induced $\Delta\Psi$ loss without altering $Ca^{2+}$ uptake. Isolated mitochondria were successively treated with 50 μM $Ca^{2+}$ (indicated by arrowheads) in the presence (pink) or absence (blue) of 1 μM CsA, and $\Delta\Psi$ (**d**) and extra-mitochondrial $Ca^{2+}$ (**e**) were monitored. **f**, Accumulation of $Ca^{2+}$ in the mitochondria as a result of CypD deficiency. Mitochondria were incubated with the indicated concentrations of $^{45}Ca^{2+}$ for 25 min and intra-mitochondrial $Ca^{2+}$ was measured. Data shown as mean ± s.e.m. **g**, Lack of $Ca^{2+}$-induced, but not rBid- and rBax-induced, cytochrome *c* release in $CypD^{-/-}$ mitochondria. WT, $Bak^{-/-}$ and $CypD^{-/-}$ mitochondria were incubated with $Ca^{2+}$, rBid, and rBax at the indicated concentrations. After 30 min, samples were centrifuged and aliquots of supernatants were subjected to western blot analysis for cytochrome *c*. 'Total' represents the total amount of cytochrome *c* found in an equivalent aliquot of the mitochondria.